Dyke-arrest scenarios in extensional regimes: insights from field observations and numerical models, Santorini, Greece

Kyriaki Drymoni[a*], John Browning[b, c], Agust Gudmundsson[a]

[a]Department of Earth Sciences, Queen's Building, Royal Holloway University of London, Egham, Surrey TW20 0EX, UK

[b]Department of Mining Engineering and Department of Structural and Geotechnical Engineering, Pontificia Universidad Católica de Chile, Santiago, Chile

[C]Andean Geothermal Centre of Excellence (CEGA), Santiago, Chile

* Corresponding author
E-mail address: Kyriaki.Drymoni.2015@live.rhul.ac.uk

Abstract

During a volcanic unrest period with magma-chamber rupture, fluid-driven fractures (dykes) are injected either from deep reservoirs or shallow magma chambers. Subsequently, the dykes follow propagation paths towards the surface, some eventually reaching the surface to erupt while others become arrested. Here we study dyke paths resulting in eruption or arrest in an excellent 5-km wide exposure of the northern caldera wall of the Santorini volcano in Greece. Mapping of more than 90 dyke segments shows that they were emplaced in a host rock consisting of layers (of breccia, tuff, scoria, and lava) with a wide variety of mechanical properties. At the contacts, some dykes are arrested or deflected and hence change their propagation paths. Here we combine the field data with numerical models to explore dyke paths resulting in (1) arrest and (2) eruption. We investigate the effect of different host-rock mechanical properties, magmatic overpressures, and tectonic loading on dyke paths. We find that layers with unfavorable local stresses for dyke propagation, namely stress barriers, result from layer stiffness (Young's modulus) contrast and thickness variations and are a common cause of dyke arrest. The study also shows how the details of the dyke path, and eventually dyke-fed eruptions, depend on the mechanical layering and local stresses in volcanoes. The results are of great importance for understanding dyke-propagation paths, and the likelihood of eruption, during unrest periods, particularly in stratovolcanoes fed by shallow chambers, such as Santorini.

KEYWORDS: dyke arrest, dyke propagation paths, Santorini Volcano, field studies, numerical modelling, mechanical layering

1. Introduction

Volcanic eruptions are typically fed by magma-filed fractures, dykes, many of which become arrested while others feed eruptions. Dykes have a variety of orientations or attitudes which relate to the local stresses controlling their formation (Anderson, 1951; Rubin and Pollard 1987; Rubin, 1995; Dahm, 2000; Gudmundsson, 2002, 2006, Burchardt, 2008; Tibaldi, 2015). To feed the eruption in the upper or top part of a volcanic edifice that stands high above its surroundings the feeder dyke must propagate vertically for at least part of its path. Many flank eruptions, by contrast, may be partly or entirely fed by laterally propagating dykes as is often the case at Etna volcano (e.g. Acocella and Neri, 2003; Scudero et al., 2019). As vertically propagating dykes approach the surface they may become arrested, some being deflected into sills (Pollard and Johnson, 1973; Geshi et al. 2010; Gudmundsson, 2011a; Barnett and Gudmundsson, 2014). Some dykes eventually reach the surface to erupt. There, is however, presently no way of predicting whether a dyke injected during an unrest period will reach the surface to feed an eruption or become arrested in the crust.

Part of the reason that this is a remaining problem in volcanology is due to the ascent path of the magma being commonly through highly anisotropic and heterogeneous crustal segments (Gudmundsson, 2011a). Field observations suggest that as little as 10-20% of dykes become feeders in stratovolcanoes (higher percentage in basaltic edifices) which are by nature highly heterogeneous (Gudmundsson et al. 1999; Gudmundsson and Brenner, 2005; Gudmundsson, 2011a). Previous studies (Lister and Kerr, 1991; Gudmundsson, 2002, 2011a; Rivalta, 2005; Kavanagh et al. 2006; Rivalta et al. 2015; Kavanagh et al. 2017; Townsend et al., 2017) have provided insights into the mechanisms that control dyke propagation and hence ultimately govern the likelihood of an eruption. Among suggested factors affecting dyke propagation are magma overpressure (Gudmundsson, 2011a,b), heat exchange between the magma and host rock (Rubin, 1995), the local stress field ahead of the dyke (Dahm, 2000), volatiles within the magma (Cashman, 2004), density and/or buoyancy (Taisne and Jaupart, 2009), the ambient deviatoric stress (Pinel and Jaupart, 2004), pre-existing crustal weaknesses (Le Corvec et al. 2013, 2018; Browning and

Gudmundsson, 2015), and crustal heterogeneity and anisotropy, which, in turn, partly control local stresses (Gudmundsson, 2011a).

In this paper we address the mechanical conditions that affect dyke-propagation paths, in particular arrest, in stratovolcanoes, using the examples of dykes in the Santorini Volcano. The main focus is on the effect of crustal layering and discontinuities between dissimilar mechanical layers on dyke propagation. We use the Finite-Element Method (FEM) through the software COMSOL Multiphysics together with data from field observations. We build model setups with realistic structural settings (attitude, thickness, host rock stratigraphy) and use calculated or literature-derived field mechanical properties (overpressure, stiffness) to gain insights into dyke propagation and arrest on Santorini volcano for the first time. The primary goal of the numerical models is to replicate the observed field structures and processes and define the likely mechanical conditions during the formation of the observed dyke path. To do this we made several model scenarios with varying magmatic overpressure for two dykes (Dyke 1 and Dyke 2) and loading conditions. In addition, we performed two suites of sensitivity tests. The first one investigated how the host rock material properties (thickness and stiffness of the layers) and the stratigraphy (the sequence of layers) associated with variable magmatic overpressure promote stress rotations that affect dyke paths. The second suite studied explicitly the relationship between the regional stress field and the varying magmatic overpressure during the formation of the Santorini dyke swarm.

2. Mechanisms of dyke propagation and arrest – previous work

Before we describe the local geology of Santorini and the dykes themselves, we give a brief overview of the current understanding of the conditions for dyke propagation and arrest. This we do so as to put the geological information, provided in later sections, into the framework of mechanics of dyke propagation in layered rocks.

Dyke arrest is common in stratovolcanoes as the layers which make up a volcano are of widely different mechanical properties (particularly as regards Young's modulus/stiffness) which promote abrupt changes in the local stress field (Gudmundsson, 2003, 2011a,b). Analytical studies (Hutchinson, 1996) and field observations (Gudmundsson, 2011a) show that when a vertical extension fracture such as a dyke meets a horizontal discontinuity such as a contact between

dissimilar layers, the extension fracture/dyke may (1) penetrate the contact, and continue its vertical propagation, (2) become arrested at the contact, or (3) become deflected or offset, and so change its path or form a sill.

Analogue and numerical modelling indicate that when a dyke passes from a soft layer to a stiff layer, the dyke commonly becomes deflected into a sill, or it can become arrested (Kavanagh et al. 2006, 2018; Gudmundsson, 2011a,b). Conversely, if a dyke passes from a stiff layer to a soft layer, then it is more likely to continue its propagation towards the surface.

The basic criterion for extension (mode I) fracture propagation derives from the work of Griffith (1921, 1924), which is partly based on stress-field calculations made by Inglis (1913). In modern notation, the criterion states that for the fracture/dyke to propagate the elastic energy release rate G should be at least equal to (or exceed) the critical energy release rate, namely the material toughness, G_{IC}, which is the energy absorbed during the fracture propagation, primarily through the formation of the fracture surfaces (dyke walls). The criterion may be stated as (Broek, 1982; Gudmundsson, 2011b):

$$G = \frac{\pi \sigma_c^2 a}{E} \geq G_{Ic} \tag{1}$$

$$\sigma_c = \sqrt{\frac{EG_{Ic}}{\pi a}} \tag{2}$$

where a is half the crack length (total length for an edge crack), E is Young's modulus, and σ_c is the failure tensile stress at the tip. Accordingly, an extension fracture/dyke propagates when sufficient energy (G) is available (released or transformed) to rupture the rock and form the fracture surfaces/walls. For dyke propagation this energy is mostly elastic energy (strain energy) stored in the volcano during unrest-related inflation (Gudmundsson, 2012).

There are three primary mechanisms related to mechanical layering that control dyke propagation and arrest (Gudmundsson, 2011a,b). These mechanisms apply to extension fractures (mode I cracks) in general but are here applied to dykes. These mechanisms are stress barriers, elastic

mismatch, and Cook-Gordon delamination (cf. Gudmundsson, 2011a,b) and are described below (Fig. 1).

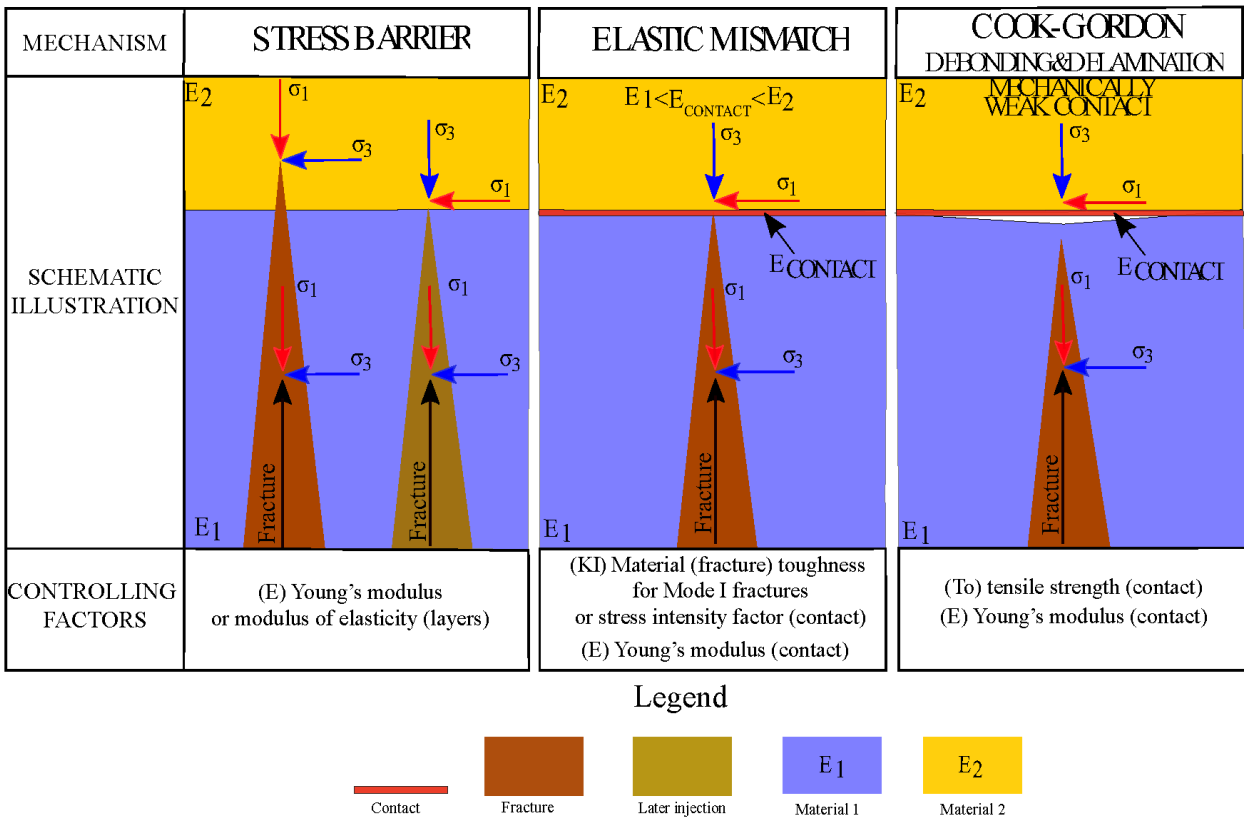

Figure 1: Schematic illustration of the three primary mechanisms (Stress barriers, Elastic mismatch and Cook-Gordon debonding and delamination) that control fluid-driven fracture arrest. In part C the weak contact delaminates and opens ahead of the progressing fracture tip. The controlling factors of each mechanism are shown at the bottom.

2.1 Stress barriers

Rotation of the principal stresses is common at the contacts between rock layers of dissimilar stiffness. Dykes are predominantly extension fractures/mode I cracks and so normally propagate in the direction of/parallel with the maximum principal stress (σ_1). When the principal stress orientations rotate at a contact, then the dyke propagation path will change accordingly. Vertical propagation can occur only if the maximum principal compressive stress σ_1 is vertical (and the minimum principal compressive stress σ_3 is horizontal), so that if σ_1 rotates to become horizontal

at the contact (and σ_3 thus vertical), the vertical dyke propagation will stop. The dyke then either becomes arrested on meeting the contact or becomes deflected into a sill along the contact.

Both stiff and soft (high and low Young's modulus) layers can act as stress barriers (Gudmundsson and Phillip, 2006; Gudmundsson, 2011a). For example, a stiff layer can become a stress barrier subject to horizontal compression which may happened following normal faulting, particularly graben subsidence, or during multiple dyke injections where the magmatic overpressure of the previous injections (Geshi et al., 2010) may have generated horizontal compression in the adjacent stiff layers. Many studies show that earlier dyke intrusions or graben formation generate horizontal compression, thereby temporary stress barriers (Gudmundsson, 2008; Menand et al., 2010). Similarly, compliant layers can become temporary stress barriers for vertical dykes when the loading is horizontal tension (Gudmundsson and Brenner, 2001).

2.2 Elastic mismatch

In a heterogeneous and anisotropic material, the presence of interfaces with different mechanical properties may encourage propagation along the interface in a mixed fracture mode (Garcia, 2014). In geology, interfaces are primarily contacts, fractures, and other discontinuities. When there is large contrast in stiffness across a contact/interface and the energy release rate (G_I) during extension fracture/dyke propagation reaches the material toughness of the interface/discontinuity then the dyke can become deflected into the discontinuity and propagate as a mixed-mode fracture (I and II) (Hutchinson, 1996; Xu et al., 2003). The mechanical properties of the discontinuities depend on the Dundurs elastic mismatch parameters α (Dundurs, 1969; He et al., 1994) that partly define the conditions for dyke penetration of, or deflection into, the discontinuity. These findings are supported both by analogue (Kavanagh et al. 2017) and rock deformation experiments (Forbes-Inskip et al. 2018).

2.3 Cook-Gordon delamination

Observations from experiments and analytical calculations show that the contact between layers can both debond and delaminate in composite materials (Cook and Gordon, 1964; Wang and Xu, 2006). This process occurs when the tensile stress at the tip of a propagating extension fracture is

sufficiently high so as to open the contact ahead. This mechanism applies also to layered rocks and is common during dyke-fed sill emplacement at shallow depths (Gudmundsson, 2011a; Barnett and Gudmundsson, 2014).

A dyke will open a contact ahead of its tip when the dyke-parallel tensile stress is large enough to overcome the tensile strength (T_o) of the contact. The dyke-parallel tensile stress is about 20% of the dyke-perpendicular tensile stress at the tip of the dyke (Freund and Suresh, 2003; Gudmundsson, 2011a). The tensile strength of a contact, particularly in an active volcano or volcanic zone, is often very low – close to zero – and thus easily opened, particularly at shallow depths. This mechanism has been studied in volcanic environments using numerical models (Gudmundsson 2003) with a specific focus on shallow depths and stiff contacts (basaltic lavas) but is also well known as a major fracture-arrest mechanism in composite materials (Xu et al., 2003; Wang and Xu, 2006; Garcia, 2014).

3. Regional field setting

3.1 Geological setting

We now turn to the geology of the Santorini Volcano, within which the dykes discussed here are located. Santorini is a Quaternary central volcano, a volcanic complex, and part of the South Aegean Volcanic Arc in Greece. The volcanic complex formed in a trans-tensional regime and has been influenced by the oblique subduction and accelerated slab rollback (Brun et al., 2017) of the African tectonic plate underneath the Aegean tectonic plate (Le Pichon and Angelier, 1979). Sinistral and dextral strike-slip zones as well as other extensional structures (faults and grabens) (Sakellariou et al. 2013) have operated since the Miocene (Grasemann et al. 2012).

The orientation of the sub-horizontal minimum compressive stress (σ_3) is N135º E (N45°W), and the level of the deviatoric regional stress tensor (deviation from the mean stress, here the lithostatic state of stress) associated with an unrest period in 2011-12 has been estimated at around 3 MPa (Feuillet, 2013). The Coulomb stress in the region increased by up to 0.5 MPa during this period, as the magma chamber received new magma and inflated (Parks et al. 2012). Although there was an increase in magma chamber pressure, the shallow chamber did not rupture or form a dyke (Browning et al. 2015).

Santorini volcano has experienced many eruptive cycles, at least four caldera collapse events, and remains active (Druitt and Francaviglia, 1992; Druitt et al., 1999). The past Plinian and sub-Plinian volcanic activity formed a complex pile of stratigraphic horizons. There have been two explosive cycles with at least 12 pyroclastic eruptions and dyke fed eruptions that produced lava shields and lava domes (Druitt et al., 1999). The volcano hosts a magmatic plumbing system whose magmas are the result of many processes such as mantle wedge partial melting, fractional crystallisation, magma mingling, mixing and crustal assimilation (Zellmer, 1999; Druitt et al. 1999; Andujar et al. 2015).

3.2 Santorini northern caldera wall

In this study, we focus on the eroded dyke swarm in the northern caldera wall of the central part of the island of Santorini between the villages of Oia (west) and Imerovigli (east) (Fouque 1879; Nicholls 1971; Puchelt 1990; Browning et al. 2015). In Figure 2 we present a simplified geological map of the island showing the main units discussed here. The dykes are emplaced in a highly heterogeneous and anisotropic host rock that belongs mainly to the oldest composite stratocone, the remnants of the Peristeria volcano, which was constructed between 530 and 430 ka (Druitt et al. 1999). The Peristeria volcano is composed primarily of andesitic lava flows, but also of basaltic and silicic lava flows, tuffs, breccias (hyaloclastites) (av1-av3) (Druitt et al. 1999). Several dykes cut through middle tuffs (ap4, 125-80 ka) and thick scoria fall deposits (ap4a-c). The Cape Riva caldera collapse structure (~21ka) formed after the construction of the Skaros shield (54 ka) and the Therasia dome complex (25 ka). Both the latter erupted andesitic and basaltic lavas, as well as thick, spatter agglomerates (as2, ap5, and ao) (Druitt et al. 1999).

The dykes do not penetrate the eruptive materials of either the 1st explosive cycle (ra, ap2, rp3) which are mainly rhyodacites (224-72 ka), or the much later Minoan fall deposits (21-3.6 ka). The caldera collapse events, and other erosional processes have exposed the stratigraphic layers, contacts and dykes, allowing them to be examined in considerable detail.

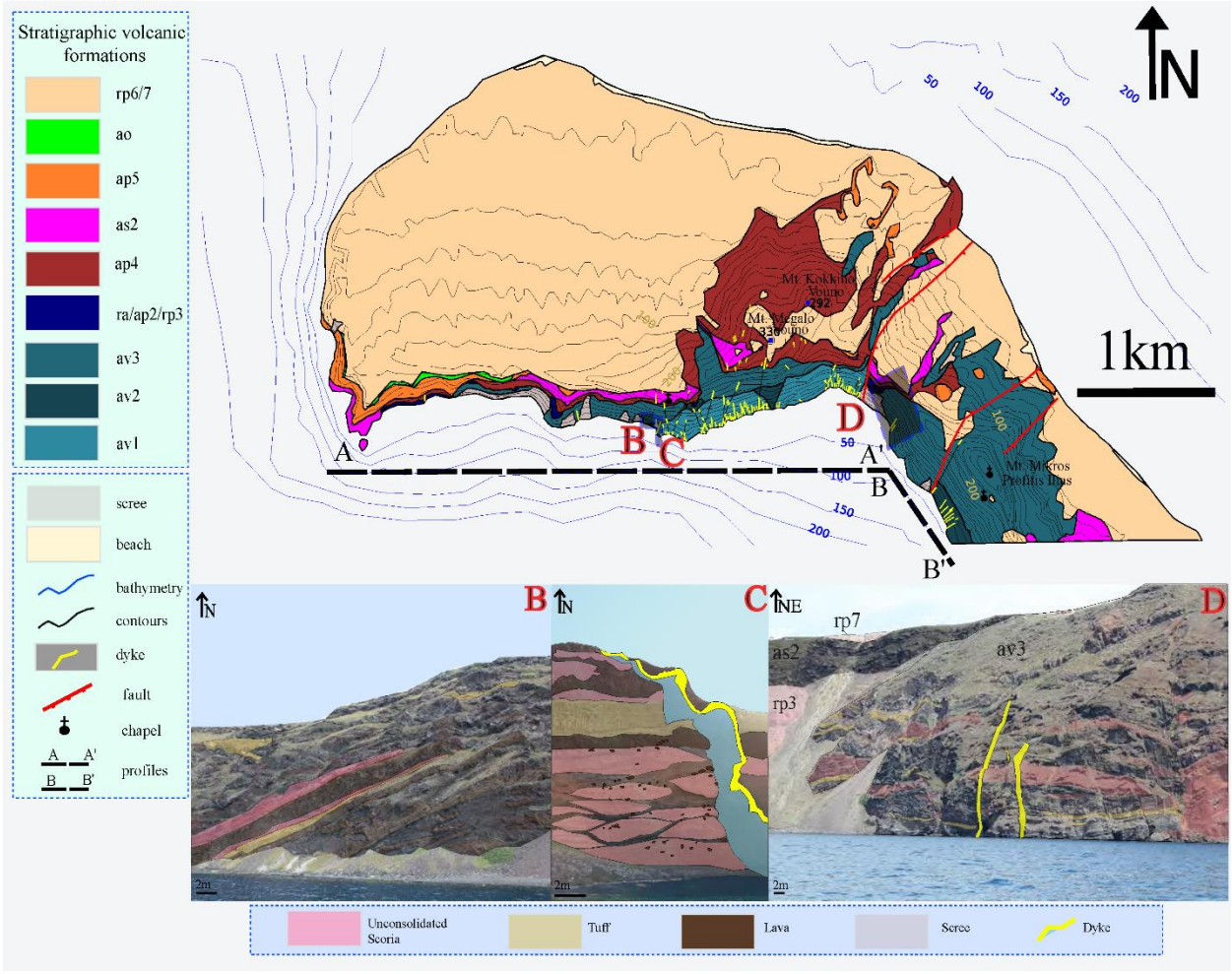

Figure 2: (A) Geological map of the northern caldera wall modified from Druitt et al. (1999), showing the location of the dyke swarm. The key on the left shows the lithologies found on the northern caldera wall (Druitt et al. 1999). Av1: andesitic lavas, tuffs, scoria and breccia, av2: silicic andesitic lavas, av3: thinly bedded andesites and basalts with subordinate dacites, tuffs and scoria, ra: rhyodacites, ap2: pink sillar facies of a pyroclastic density current and red spatter agglomerate with abundant plutonic nodules, rp3: rhyodacitic pumice, ap4: middle tuffs thick scoria-fall deposits, as2:andesites and basalts of Cape Skaros, ap5: upper scoria 2- andesitic thick spatter agglomerate, ao: andesites of Oia, rp6: Cape Riva tuff, rp7: Minoan tuff. Cross sections along the caldera profile: (B) panorama of the northern caldera wall, the av3 horizon, annotations mark the horizons of andesitic lavas, tuffs and scoria, (C) a dyke that cuts through a heterogeneous segment which exhibits anastomosing textures at the base, annotations mark the horizons of andesitic lavas, tuff and scoria (D) panorama close to the NE corner of the caldera wall, the dykes were arrested

or deflected within different layers (and hence at different depths) in the heterogeneous host rock, which is comprised of tuffs, scoria and lavas.

4. Material properties and methods

4.1 Material properties

The observed dykes propagate through layers with different Young's moduli (E). Young's modulus generally increases with depth in the crust but decreases with increasing host rock porosity, temperature, weathering, and fracture damage (Ray et al. 2006). It is worth noting that E values that are derived from static laboratory measurements are often significantly higher than the ones measured in-situ (Gudmundsson, 1988; Bell, 2000) and the difference between the two measurements can be as much as 20-65% (Ray et al. 2006). E values generally range between 10-40 GPa for basement rocks (Gudmundsson, 2011b) and between 1-15 GPa for shallow crustal rocks (Ray et al. 2006; Becerril et al. 2013), although in active volcanic areas layers of pyroclastics and sediments may have E values as low as 0.1 GPa or, occasionally, 0.01 GPa (Heap et al. 2019).

For the modelling setups, we used realistic material properties (cf. (Gudmundsson, 2011a,b). For compliant materials such as tuffs, unconsolidated scoria and breccia (hyaloclastites) we used the values of 5 GPa, 0.08-0.5 GPa and 0.1 – 8 GPa. For stiff materials, such lava flows we used the values of 10 GPa. We gave all the rocks a constant Poisson's ratio of 0.25 (Babiker and Gudmundsson, 2004) and density values of ρL=2600 kg/m^3 for the lava flows and ρT= 2000 kg/m^3 for the tuff and scoria layers. For all the models we used the stiffness ratio contrasts of the studied contacts which were defined as the dimensionless ratio (r) E_U/E_L where E_U is the Young's modulus of the upper layer and E_L is the Young's modulus of the lower layer.

4.2 Field methods

We carried out field campaigns at Santorini volcano and mapped sections of the northern caldera wall with a specific focus on the dyke swarm, as well as the associated lavas and eruptive units. The dyke swarm in the area extends through two profiles, profile 1) A-A' which is 4 km long and profile 2) B-B' which is 1.5 km long (Fig. 2). The profiles were studied both offshore (from a boat)

and onshore. The location (longitude/latitude), attitude, thickness (width) of each dyke was recorded as well as host rock lithologies, observed dyke pathways, cross-cutting relationships, and exposed length (where possible).

4.3 Numerical modelling methods

The numerical models were made using the finite element method (FEM) program COMSOL Multiphysics (v5.2). The Structural Mechanics module allows the analysis of static stresses and strains resulting from a set of imposed boundary conditions and solid-mechanical properties. Dynamic boundary loads can be simulated by altering both the magnitude and orientation of loads and hence simulate 2D deformation processes of fractures and rock units with geometrical complexity.

In our numerical models we assign different levels of Young's modulus (stiffness) to a series of mechanical units based on the field observations. The differences in Young's moduli between units generates elastic mismatch. We consider the assigned amount of mismatch and plot the resulting stress distribution (contour surface) and principal stress orientation (arrow surfaces) to assess how the level of mismatch alters the crustal stresses and influences fracture propagation. As we are interested in dyke propagation, we plot the concentration of tensile stresses at the dyke tips. It is now well known that the range of tensile stress should be between 0.5 to 9 MPa (Amadei and Stephansson 1997; Gudmundsson, 2011b) for the fracture to grow or propagate. Hence, a criterion (Dundurs, 1969; He et al., 1994; Gudmundsson, 2011b) between the elastic mismatch between layers and the amount of stress can be generated and this is what is evaluated from the models which in turn reflect the field observations.

4.3.1 General model setup

The 2D models were designed to investigate how the orientation and magnitude of stresses change as a dyke propagates through mechanically dissimilar layers and also what effect a regional extension has at the distribution of stresses. The modelling procedure is as follows. Initially, we imported the geometries of the observed geological structures into the models. Each dyke was modelled as an elliptical cavity with internal overpressure. Each layer of the models was assigned material properties (Young's modulus, Poisson's ratio, and density) and boundary loading

conditions on the horizontal edges to simulate extension. For all the models we kept the lower boundary fixed while the upper boundary is a free surface (i.e. a surface free from shear stress and constraints). We generated a triangular mesh of maximum nodal lengths <0.306 m and checked to ensure that the modelled area of interest was sufficiently far from the model edges so as not to be contaminated by edge effects.

4.3.2 Baseline model setup

In Figure 3 we present the setup for a suite of baseline models used to test to later models that simulated more complex geometry. In the baseline model (Fig. 3A), we simulated a dyke with 5 MPa overpressure in a homogenous crustal segment. In Figure 3B the model geometry is identical but with an added extra layer atop with a Young's modulus of 10GPa. In Figures 3C and 3D we show the same baseline models as in Figs. 3A,B but add an additional horizontal loading extension of 0.5MPa to simulate an extensional stress field.

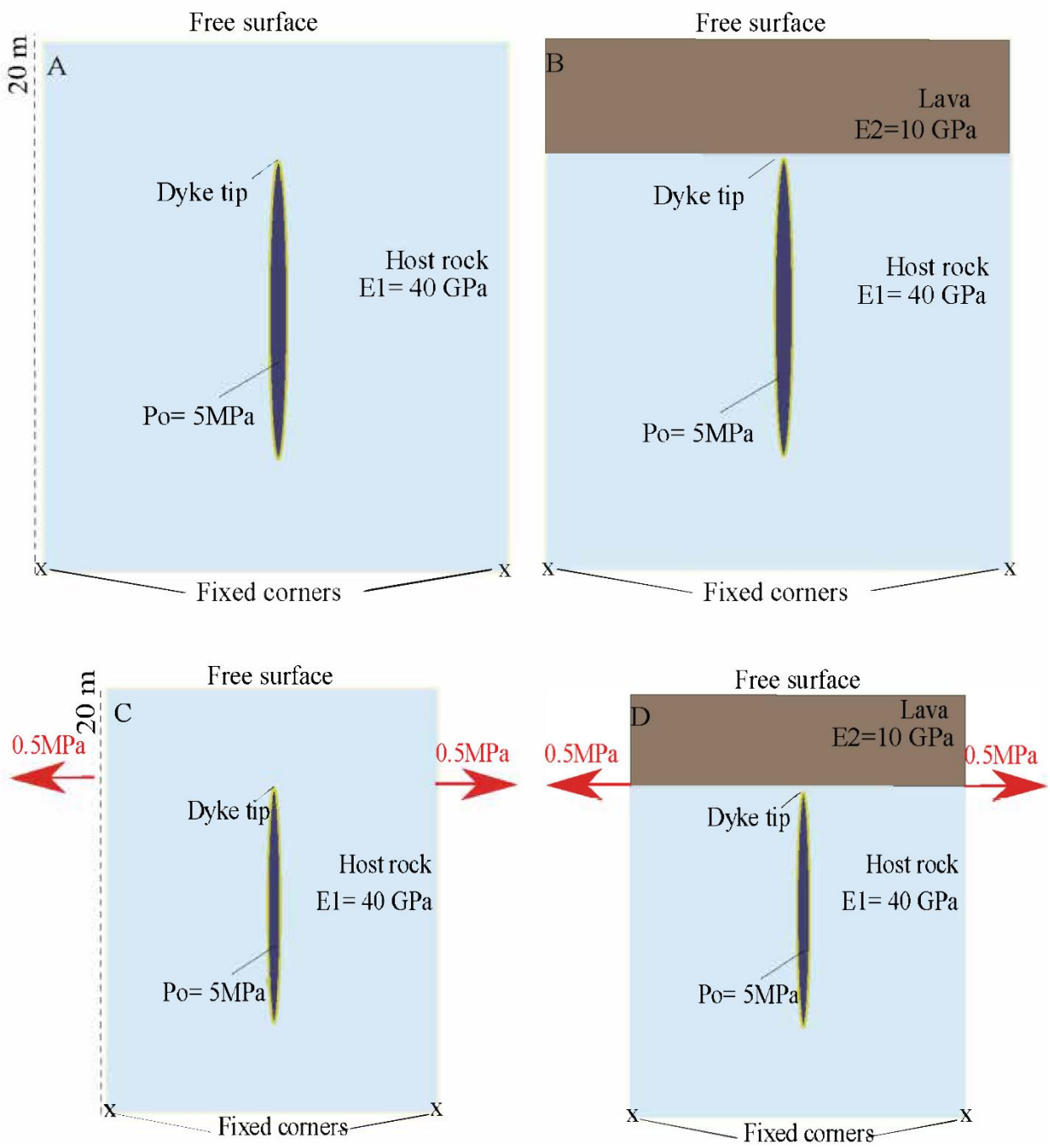

Figure 3: Four model setups. (A) Homogeneous host rock with Young's modulus of 40 GPa and a 1 m thick cavity (dyke) with an internal pressure of 5 MPa (B) Example of a 2 layered or heterogeneous model with a Young's modulus of 40 GPa in E1 and a Young's modulus of 10 GPa in E2, again with a 1 m thick dyke (C) Homogeneous host rock with a Young's modulus of 40 GPa and a 1 m thick cavity (dyke) with an internal pressure of 5 MPa subjected to an extra horizontal extension of 0.5 MPa at the boundaries. D) Example of a two layered or heterogeneous

model with a Young's modulus of 40 GPa in E1 and a Young's' modulus of 10 GPa in E2, again with a 1 m thick dyke and subjected to an extra extensional force of 0.5 MPa (denoted by the red arrows).

4.3.3 Modelled field example model setup

We measured 91 dyke segments in this part of the caldera wall of Santorini. Of these we selected two that had exceptionally clear paths for modelling (Fig. 4). While we particularly model these two dykes, the results are general and apply to other dykes as well – these were simply selected because they are so well exposed.

The two dykes, hereafter referred to as dyke 1 and dyke 2, are compositionally identical, both being basaltic andesites (Bailey et al., 2009), have similar attitude and average thicknesses, and propagated through essentially the same host-rock stratigraphy. We identified five distinct dyke populations through analysis of petrological data and attitude on Santorini. The two dykes belong to the same dyke population and were likely injected from the same magma chamber. We assume that the dyke propagation paths follow the direction (or trajectory) of σ_1, as is normal (Gudmundsson, 2006, 2011a).

All the models reflect snapshot simulations of the magnitudes and directions of the stress field around the dykes and the host rock. For the interpretation of the results, we plot the magnitudes – the contours – of maximum tensile stress (σ_3), on a two-dimensional surface to examine stress concentration at the dyke tips. The contours show the location of the highest stress concentration and their ranges in different type of contacts. We also plot the trajectories of the maximum principal compressive stress (σ_1) and the minimum principal compressive stress (σ_3) in all the models.

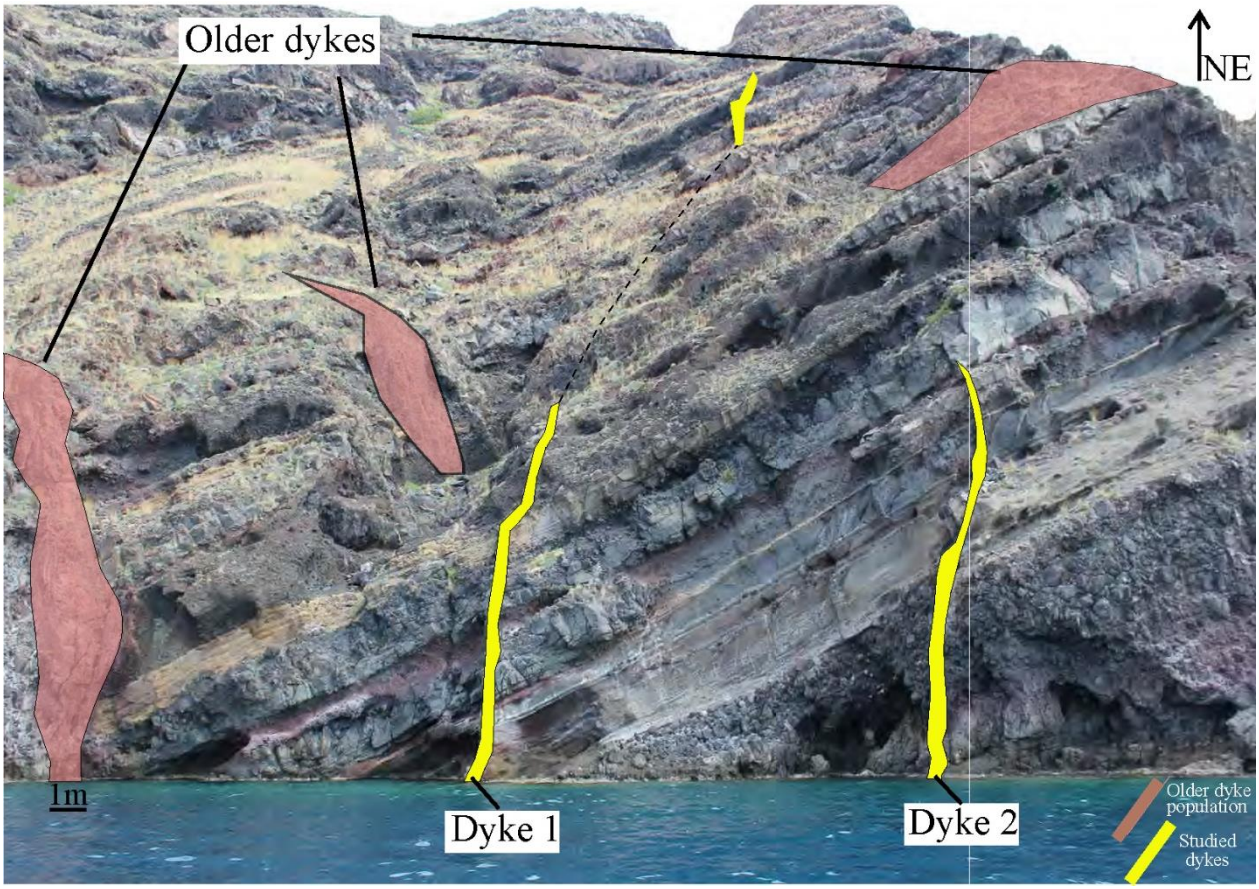

Figure 4: Studied dyke 1 and dyke 2 (annotated yellow) in the northern caldera wall. Older dyke populations (annotated pink) can also be observed in the cross-section.

4.3.4 Sensitivity tests

The first round of sensitivity tests provides insights into the effects of stratigraphy and mechanical properties for different loading conditions on stress rotations (stress barriers). For dyke 2 we made the following tests to explore this effect:

1) Increasing the thickness of a lava flow by an order of magnitude (from 1 to 10m).

2) Increasing the thickness of a scoria layer by an order of magnitude (from 1 to 10m).

3) Alternating the layer sequence.

4) Increasing the thickness of the crustal segment above the dyke (more layers on the top of the observed stratigraphic sequence).

We made these sensitivity tests (1,2,4) for the same two overpressures in the dyke, namely alternatively 1 MPa and 5 MPa, testing the same contact (E2 (tuff) / E1 (breccia)) by keeping the tuff stiffness constant (E2=5GPa) and changing the stiffness of the breccia layer from very compliant (0.1 GPa), to compliant (1 GPa), and ,finally, to comparatively stiff (10 GPa). The performed ratios of stiffness were respectively: E_U/E_L= 5/0.1 =50, E_U/E_L= 5/1 =5 and E_U/E_L= 5/10 =0.5.

For the alternative layer sequence (sensitivity test 3) we tested for the same two overpressures in the dyke, namely alternatively 1 MPa and 5MPa, using the contacts (E2 (scoria) / E1 (breccia) and keeping the scoria stiffness constant (E2=0.5GPa) while changing the stiffness of the breccia layer from very compliant (0.1 GPa), to compliant (1 GPa), and finally to comparatively stiff (10 GPa). The performed stiffness ratios were respectively: E_U/E_L= 0.5/0.1=5, E_U/E_L= 0.5/1 =0.5 and E_U/E_L= 0.5/10 =0.05.

For the second round of sensitivity tests, the models focused on the relationship between the magma chamber loading conditions and the regional stress field subject to different material properties of the breccia layer (i.e., 0.1 GPa, 1 GPa, and 10 GPa), as above, and testing the same contact ((E2 (tuff) / E1 (breccia)). These models allow us to investigate whether the stress rotations relate to the regional extensional stress regime or to local stress effects, such as due to dyke-induced compression. Six different loading conditions that reflect 6 tested distinct stress fields are presented below:

S1: Horizontal extension of 1MPa - benchmark model.

S2: Magmatic overpressure of 1 MPa – simulating dyke conditions close to a magma chamber.

S3: Magmatic overpressure of 1MPa and horizontal extension of 3MPa – simulating a dyke emplaced in a rift zone (or, as possible for Santorini, an accelerated slab retreat).

S4: Magmatic overpressure of 1MPa and horizontal extension of 0.5MPa – simulating a dyke emplaced in a rift zone.

S5: Magmatic overpressure of 1MPa and horizontal compression of 3MPa –simulating a dyke emplacement following recent previous dyke injections.

S6: Magmatic overpressure of 1MPa and horizontal compression of 0.5MPa – simulating a dyke emplacement that is subject to a tectonic event, here graben subsidence or formation.

For all the models, three arrow surfaces were used to express the principal stresses for better visualisation of the stress field. Here the maximum principal compressive stress (σ_1) is shown by red arrows, intermediate principal stress (σ_2) by white arrow and the maximum tensile stress (σ_3) by black arrows. The loading condition is again magmatic overpressure. The original models are included in the supplementary files (Supporting information files 1-6).

5. Field results

We obtained structural data on 91 well exposed dyke segments observed in the northern caldera wall of Santorini island. These data were combined and compared with previous measurements by Fouque (1879), Petersen (2005), and Browning et al. (2015).

5.1 Dyke attitude and thickness

Regional dyke swarms usually show normal-curve strike and dip distributions, being mostly composed of sub-vertical and subparallel dykes that consequently, seldom cross-cut (Gudmundsson, 2002). In Santorini, dyke propagation is thought to have been primarily vertical from a shallow magma chamber (Browning et al., 2015). The present field observations provided indications of vertical flow such as elongated vesicles parallel to the dip dimension but no elongated minerals as the dykes are often aphyric or plagioclase crystals are the only phenocrysts. The dykes are primarily perpendicular to the regional direction of σ_3, which coincides with the direction of the spreading (or rifting) vector or defined by the elongation of the caldera collapse (Gudmundsson, 2006). The great majority of the dykes are subvertical. More specifically, 91% have dips >75degrees; the few dykes (9%) that dip 45-60 degrees can be then categorised as inclined sheets (Fig. 5C). Since the dykes are mostly derived from a shallow chamber, we assume the dip dimension (height) to be the controlling (smaller) dimension.

The predominant strike is in the range N20-45ºE, but there are also other minor sets of N-S, (between N0-20ºE) and NW-SE striking dykes (Fig. 5A). The variation in frequency of dykes along the profile shows that the dykes occupy four distinct localities. We infer that these localities mark the boundary between at least two of the main historical eruptive centres (cinder cones) in

the northern part of Santorini, namely Mt. Megalo Vouno (or Mavro Vouno), Mt. Kokkino Vouno as well as two other localities such as the Mt. Mikros (or Chamilos) Profitis Ilias and the village of Finikia (Fig. 5B).

Field measurements suggest that the length and thickness size distributions of dykes are normally power laws (Gudmundsson, 1995). Dyke thicknesses in Santorini range from 0.1m to 8 m with an arithmetic average thickness of 1.1m. Field observations have shown that in some cases the dyke thickness varies along both the strike and dip dimension of the same dyke (or segment). In Fig. 5D we show how dyke thickness varies along with each profile and in Fig. 5C we show the variation in dyke thickness with dyke dip.

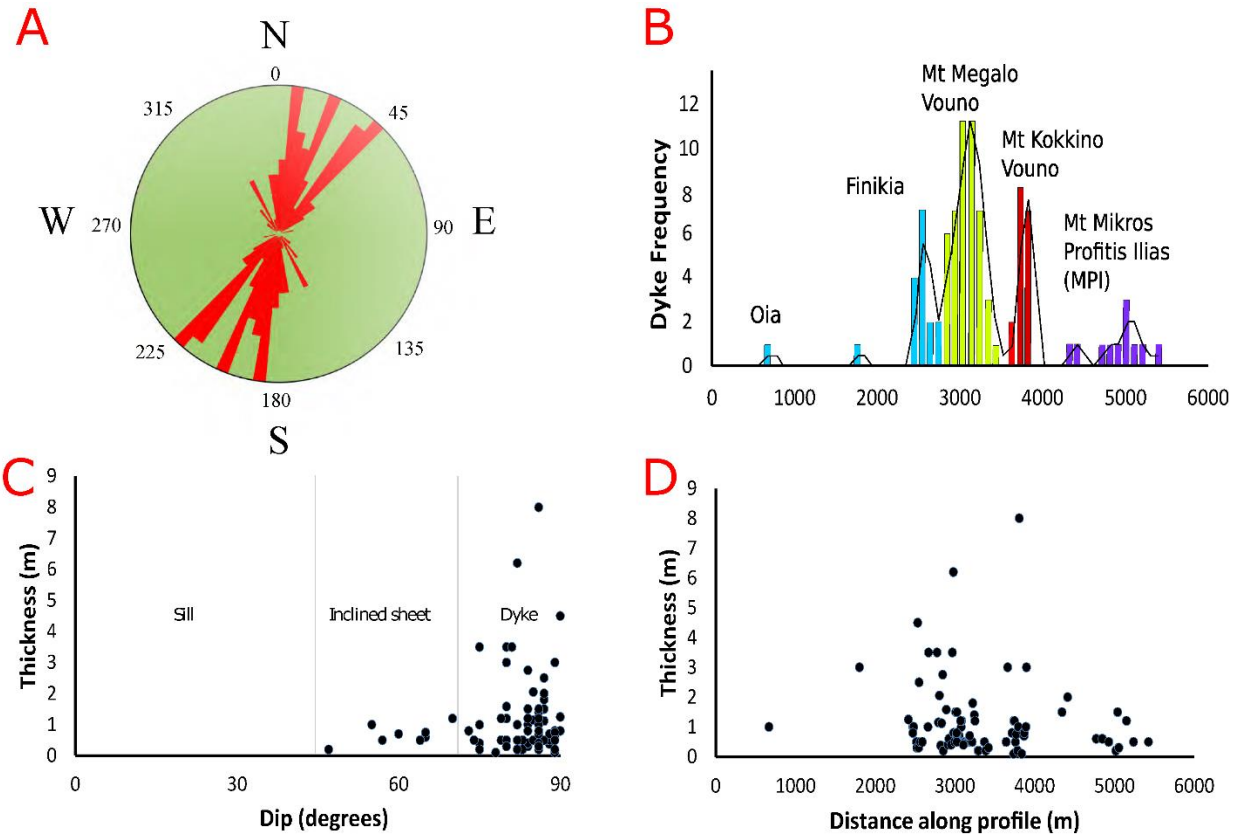

Figure 5: Characteristics of the dykes exposed on the Santorini northern caldera wall. (A) Rose diagram of dyke strike directions, (B) Frequency of dykes along the profile, (C) Dyke thickness as a function of dyke dip, D) Thickness of dykes along the measured profile.

5.2 Dyke attitude, deflection and arrest

Dyke attitudes vary both along the length of the profile and also with depth in the caldera wall. During the field campaigns, we collected measurements of dyke attitudes from a distance along the profiles as we could not directly measure the along dip variations because the caldera wall was too steep and difficult to access in many sections. For that reason, we made many qualitative observations on how the dyke attitudes change along dip. The observed criteria were:

- Propagation/feeder: the dyke penetrates the host rock, and its segments were visible throughout the succession. Because the top parts of the dyke are then essentially at the surface (which is only slightly eroded), it is highly likely that the dyke fed a volcanic eruption. We do not see direct evidence for this except 2 dykes that could have been connected to crater cones.

- Uncertain fate: the dyke changes attitude with depth, and we do not observe any of the dyke segments at higher levels in the succession exposed in the caldera wall.

- Arrest: the dyke is clearly arrested, and the arrested dyke tips can be observed. In this case, the dyke did not feed an eruption in the observed section.

- Deflection: the dyke changes dip and deflects into pre-existing weaknesses (faults) and either becomes arrested in a pre-existing fault zone or propagates through the fault and then becomes arrested higher up in succession. In all of these cases, it is unclear if the dyke has fed an eruption.

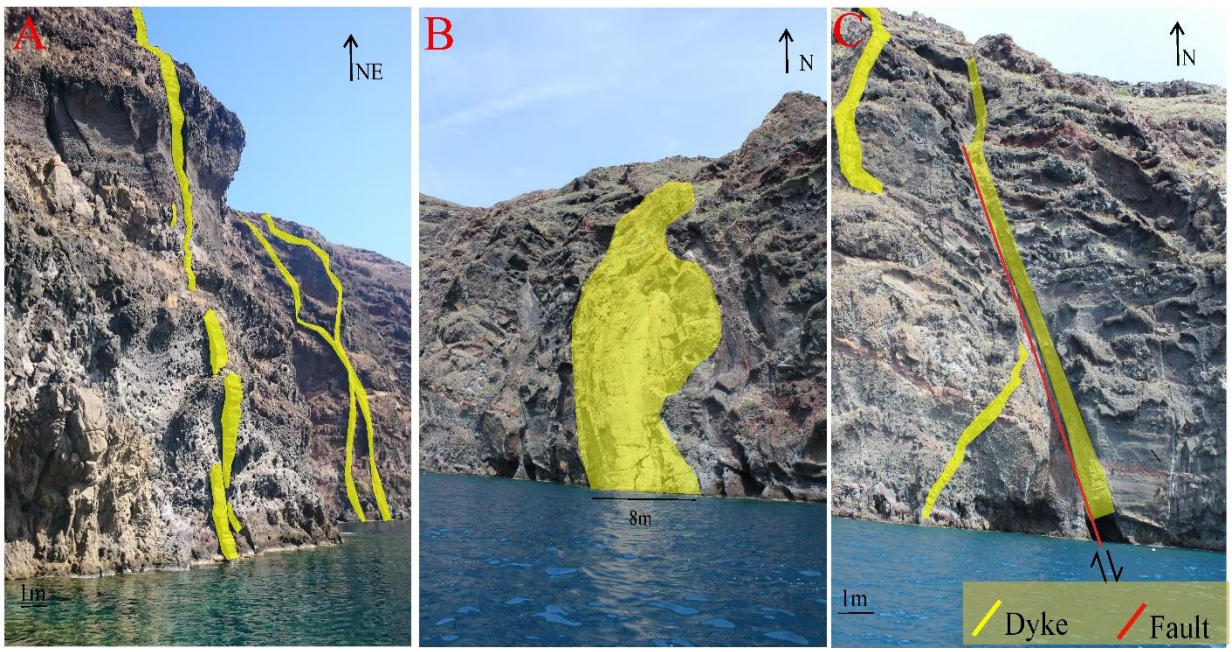

Figure 6: Observed dyke propagation paths on the northern caldera wall. (A) Segmented and branched propagated dykes, (B) a possibly multiple arrested dyke which forms rounded tips as it propagates through a compliant host rock, (C) dyke-fault deflection; the inclined sheet on the left is being deflected into the shear fracture, the normal fault.

The studied dykes broadly follow three different propagation patterns, namely:

1) Propagation: the dyke penetrates the host rock layers and follows the direction of the stress field active during emplacement. Of the 91 dyke segments measured we observed 43 dykes that penetrate all the host-rock layers and were thus apparently neither arrested nor deflected along contacts (Fig. 6A). Due to the steep cliffs, erosion, and coverage by scree and vegetation the segmented dykes cannot be followed as continuous structures up their dip dimension to the top of the succession.

2) Arrest: we observed three clearly arrested dykes. The arrested tips occur at bedding planes in volcaniclastic rocks and at contacts between lava flows. The dykes that propagated into soft volcaniclastics developed rounded tips (Fig. 6B) or thinned out - tapered away - to a pointed tip or became arrested with a blunt-ended tip at the contact between layers of different stiffness. The geometry of the tips plays a vital role in the mechanism that controls their paths (Gudmundsson, 2003).

3) Deflection: we observed six dykes that became deflected along discontinuities, which they then followed as parts of their propagation paths. We regard a dyke as deflected when the dip changes more than 30°. All the deflected dykes occur close to normal (regional) faults (Fig. 6C).

5.3 Dyke lengths

Due to the multiple caldera collapse events and the dynamic changes in Santorini's morphology, absolute dyke lengths are difficult to measure or estimate. Additionally, the caldera floor is under the sea, and the vertical caldera cliffs are difficult to climb to study the details of the dyke segmentation. Due to these limitations, it was not possible to trace individual dykes continuously for any long distances along strike, and so exact measurement of dyke length (and dyke height as well) was not possible. Instead, we inferred the length of dykes from the available outcrops.

Many previous studies have attempted, with varying degrees of success, to estimate the lengths of dykes in the field, both those found in well-exposed swarms (Gautneb et al. 1989, Gudmundsson 2003) as well as during emplacement (e.g. Jousset et al. 2003). The lengths (strike dimensions) of feeder dykes close to the surface can be inferred from the lengths of the volcanic fissure to which they supply magma (Gudmundsson, 1995). For the length of dykes at greater depths in the crust (in eroded dyke swarms) Gudmundsson (1983) measured the minimum lengths of five dykes in the eastern part of Iceland and found that they ranged from 4 km to more than 22 km. The uncertainty in length was primarily because the lateral ends/tips of some of the dykes were not exposed. Other data from feeder dykes in El Hierro, Canary Islands, revealed near-surface lengths from 75 m to 535m (Becerril et al. 2013) while in continental flood basalt provinces estimated dyke lengths vary from around 1 km to 80 km (Ray et al. 2006).

5.4 Dyke overpressure calculations

In the simplest case, a magma-filled fracture (a dyke) is initiated once the excess pressure (P_e, pressure above σ_3) in a magma chamber and the lithostatic stress or pressure (P_l) reach the in-situ tensile strength (T_o) of the host rock surrounding the chamber plus the minimum principal compressive stress (σ_3) (Eq.3). The value of P_e for chamber rupture is roughly equal to the in-situ tensile strength T_o of the host rock (the chamber roof, normally) which is generally in the range from 0.5 MPa to 9 MPa (Amadei and Stephansson 1997) but is most commonly 2-3 MPa (Gudmundsson 2011a). Thus, magma-chamber rupture occurs when:

$$P_1+P_e = \sigma_3 +T_o \quad (3)$$

The overburden pressure or vertical stress σ_v (overlying host-rock pressure) as defined as:

$$\sigma_v=\int_0^z \rho_r (z)\, gdz \quad (4)$$

where z is the vertical coordinate axis (depth in the crust below the surface), g the gravity acceleration (9.81 m s^{-2}) and ρ_r (z) the density of the overlying material as a function of depth. When the state of stress is lithostatic, then the horizontal principal stresses are equal to the vertical

stress given by Eq. (4), which is also a principal stress (cf. Jaeger and Cook, 1979; Gudmundsson, 2011a).

Analytical and numerical models (Gudmundsson, 2006; Gudmundsson and Phillip, 2006) show that the minimum principal compressive (maximum tensile) stress (σ_3) generally decreases substantially with distance from the magma chamber/reservoir. This situation dictates that dykes are may become arrested on their way to the surface, while actual arrest depends much on the mechanical layering. Combining Eq. (3) and Eq. (4), we can provide a formula to calculate the magmatic overpressure (P_o), which is the magmatic pressure or driving pressure in excess of the normal stress σ_n on the fracture plane. For a dyke that follows the trajectory of σ_1 and is therefore an extension fracture (mode I crack), σ_n must be σ_3. Once the dyke-fracture is initiated, it propagates away from the chamber and is driven by the magmatic overpressure (P_o), given by:

$$P_o = P_e + (\rho_r - \rho_m)\, gh + \sigma_d \qquad (5)$$

where h is the height of the dyke above the magma chamber (or reservoir), $\rho_r - \rho_m$ denotes the difference in density between the host rock and the magma and as such is a major contributor to buoyancy, and σ_d is the difference between the maximum (σ_1) and minimum (σ_3) principal compressive stresses in the host rock at the depth where the dyke tip is located at that moment (for a propagating dyke) or the depth of exposure below the original surface (for a solidified dyke in an eroded area).

The overpressure can also be found from the maximum dyke thickness (aperture) W and its controlling dimension L through the equation (Gudmundsson, 2011b, Becerril et al. 2013) initially derived by Sneddon (1946):

$$Po = \frac{W\,E}{2(1-v^2)L} \qquad (6)$$

where E is the Young's modulus of the host rock, v is the Poisson's ratio of the host rock, L is the strike dimension (length) of the dyke, and the other terms are as defined above. The aspect ratio W/L can be used to calculate the overpressure in the dyke (Gudmundsson, 1983; Delaney et al. 1986).

5.5 Magmatic overpressure results

We used Eq. (6) to determine the range of overpressures that propagated the studied dykes (Fig. 7) during emplacement. The results allow us to pick the most appropriate overpressure values for the numerical models. Furthermore, the results show that the overpressure responsible for dyke formation does not depend on location within the dyke swarm; the greatest variation or range in overpressure is simply where the dyke intensity (number) is highest (Fig. 7). For the calculations we used the value of 5 GPa for Young's modulus (E) of the shallow crust, an appropriate value of 0.25 for Poisson's ratio (ν), and the measured thickness of the dykes. For the length dimension, we used the 1:1500 ratio for thickness/length, as is commonly measured in the field (Gudmundsson, 2011a). The resulting magmatic overpressures range from 0.1 to 113 MPa (Fig. 7), with an arithmetic mean overpressure of about 5 MPa. Of course, if the Young's modulus used were 10 GPa rather than 5 GPa, then the mean calculated overpressure would be about 10 MPa. But the dykes are measured at very shallow depths, so that 5 GPa may be more appropriate than 10 GPa. 90% of the dyke overpressures range between 0.1 and 6MPa which agrees well with previous field studies (Gudmundsson, 2011a) and the conditions for rupture (in-situ tensile strength). More specifically, the results indicate that the dykes generally had low overpressure at the very shallow depths where they are exposed, as expected from mostly mafic dykes injected from a shallow magma chamber, as is the case for Santorini.

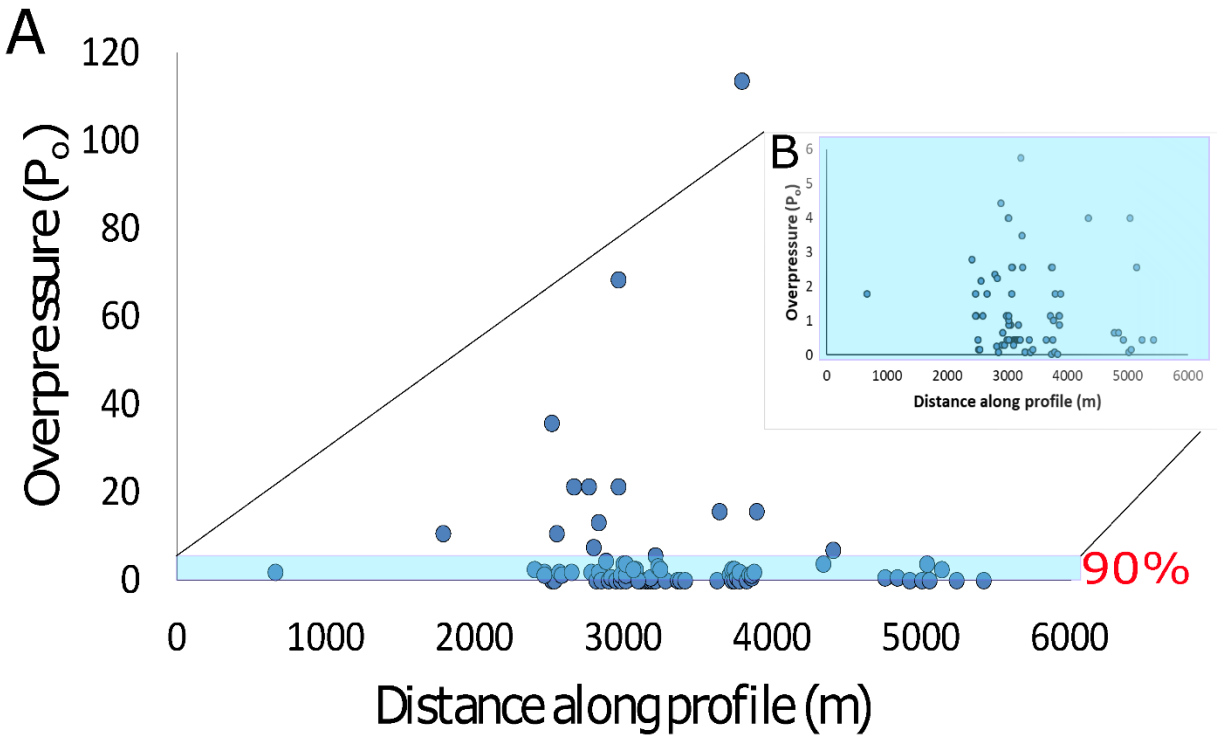

Figure 7: (A) Diagram showing the calculated dyke overpressures (P_o) with distance along the studied profile. (B) 90% of the measurements range between 0.1-6MPa.

6. Numerical modelling results

We modelled two dykes observed in the field which were of similar compositions and located within 10 m of each other. The dykes are of similar thickness and strike (NW-SE) and emplaced in the same layered rock mass with no active faults that could alter the local stress field and encourage dyke deflection (Le Corvec et al. 2013, 2018; Browning and Gudmundsson, 2015). The geometry of the rock layers dissected by the two dykes is essentially identical, but the detailed sequence, material properties, microstructure (grain sizes) and layer thicknesses, are different.

The segmented dyke 1 penetrates vertically the caldera wall and exhibits no sign of arrest in the exposed vertical cross-section. Whilst dyke 2 is geometrically and compositionally similar it has clearly become arrested within a contact between soft scoria and a stiff lava layer. The primary

goal of the numerical models was to investigate which parameters control these contrasting dyke paths.

We also studied the level of stress near the tip of each dyke and at the contact between layers ahead of each dyke. 1) very compliant - compliant (r=0.1), 2) very compliant-stiff (r=0.05), 3) stiff - very compliant (r=20) where r denotes for the stiffness contrast between two layers (E_U/E_L) (Kavanagh et al., 2006).

6.2 Dyke 1

In the results from the following models, we concentrate on the specific field example of dyke 1 and use the field measured geometries as input for a suite of numerical models. Dyke 1 is a mafic dyke with an attitude of 025/85E and an average thickness of 0.5 m (Fig. 8A). The host rock through which the dyke propagates in the exposure consists of 6 layers. Using the results from our in-situ study and those of Druitt et al. (1999) we identify them as basaltic or andesitic lavas (layers E4, E6, and E8), tuffs (layers E2 and E7), and unconsolidated scoria (layers E3 and E5). The breccia (E1) is not seen in the field but underlies all of the starting layers in the models.

We produce 2D snapshots of the dyke stresses very close to three mechanically different contacts which were selected according to the observed stratigraphy so as to favour contrasting stiffnesses and marked in Figure 8B as stars. We also simulated two loading boundary conditions. The three contacts were as follows:

Contact 1: scoria (E3 = 0.5 GPa) - tuff (E2 = 5 GPa) –/ very compliant-compliant, E=0.5/5, (r=0.1).

Contact 2: scoria (E5 = 0.5 GPa) - lava (E4 = 10 GPa) –/ very compliant-stiff, E=0.5/10, (r=0.05).

Contact 3: lava (E6 = 10 GPa) - scoria (E5 = 0.5 GPa) –/ stiff - very compliant, E=10/0.5, (r=20).

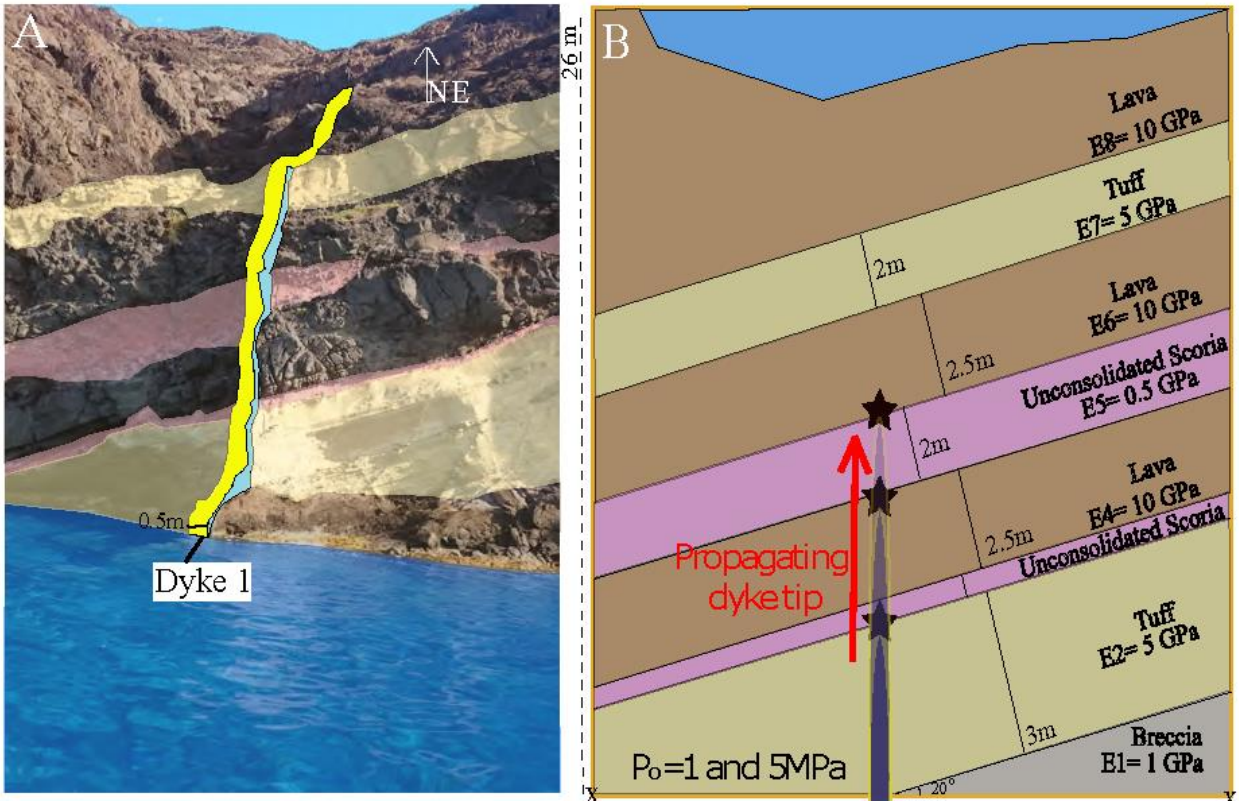

Figure 8: Dyke 1 propagated through a heterogeneous segment of tuff, unconsolidated scoria and lava in the northern caldera wall of Santorini. (A): annotated field photograph, (B): corresponding FEM model setup. The stars correspond to the specific picked contacts from which 2D snapshots were produced in COMSOL Multiphysics as the dyke is propagating towards the surface.

6.2.1 Dyke 1 with a 1 MPa driving pressure

We modelled dyke 1 with 1 MPa driving (over) pressure (P_o) as the only loading and studied the stress concentration at the dyke tip on the contacts mentioned above (Fig. 9, A1a-c). We then performed the same model runs with added regional horizontal extension of 0.5 MPa (Fig. 9, B1a-c). The model runs are shown in Fig. 9 and the results in Table 1. In Fig. 9 the stress shown as contours is the minimum principal compressive stress (σ_3) which is the maximum tensile stress, and the arrow surfaces express the maximum principal compressive stress (σ_1) (red arrows) and the minimum principal stress (σ_3) (white arrows) respectively.

In model A1-a (Fig. 9) the dyke tip tensional stresses are concentrated predominantly in the tuff (E2) and scoria (E3) units. The trajectories of the maximum principal compressive stress (σ_1) are

oriented along the dyke dip dimension, i.e. vertically, indicating that the propagation path in this model would tend to be vertical. In model A1-b the tensional stress is concentrated within the lava flow (E4) and only slightly in the overlying scoria (E5) unit. The trajectories of σ_1 are oriented sub-vertical directly above the dyke tip and thus promoting further (sub-vertical) propagation. Near the tip, however, σ_1 dips between 0° and 45° within a few tens of cm up to the next contact between the scoria (E5) and lava (E6). This suggests that if the dyke could penetrate the contact between scoria (E5) and lava (E6) it would propagate vertically for some tens of centimetres and then likely become deflected (inclined). In the next set of unit contacts (A1-c) the tensional stresses are concentrated above the dyke tip in the stiff lava (E6) unit and the trajectories of σ_1 are mainly vertical.

In model B1-a and B1–b the dyke tip tensional stresses and the trajectories of σ_1 follow similar patterns with A1-a and A1-b, although in the latter, σ_1 stays almost vertical. However, in the next unit or layer contacts (B1-c), the tensile stresses again concentrate above the dyke tip in the stiff lava (E6), but σ_1 is vertical which indicates a high likelihood of propagation as in A1-c.

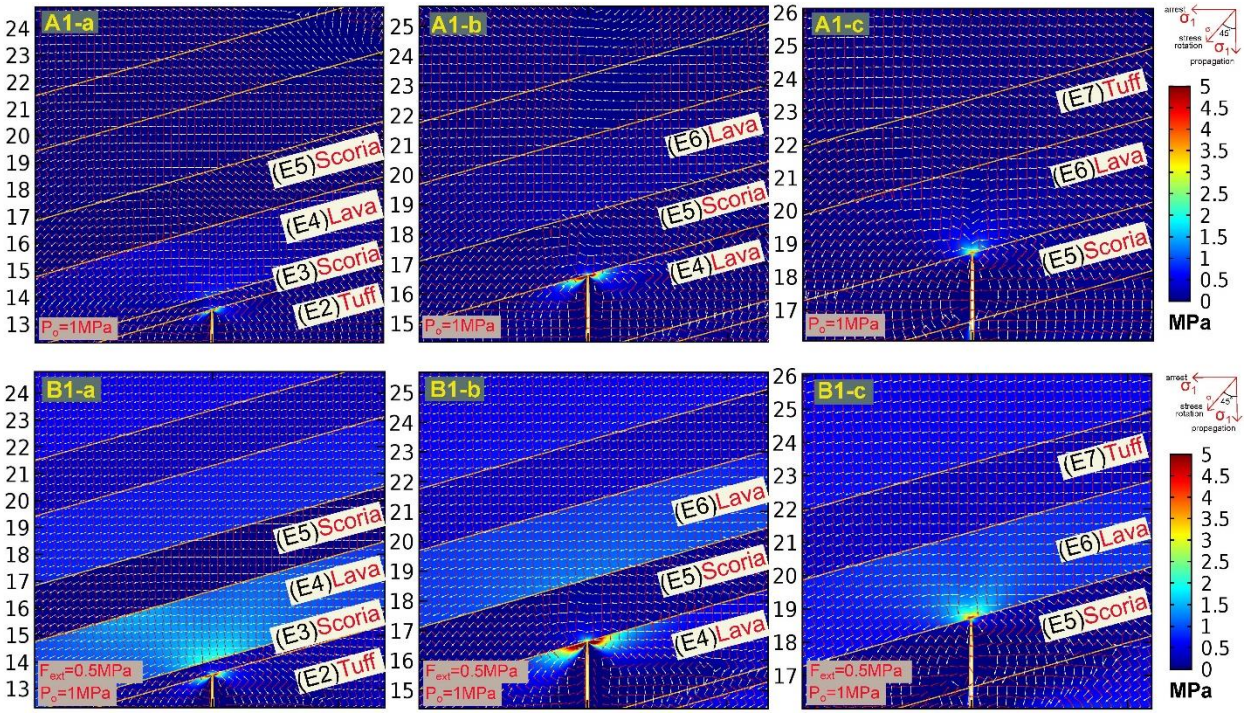

Figure 9: FEM (finite element) models of dyke propagation (tensile stress σ_3) through a heterogeneous host rock based on Fig. 8B. (A1a-c): Overpressure (P_o=1MPa) is the only loading boundary condition, (B1a-c): Overpressure (P_o=1MPa) and an extensional stress field

(F_{ext}=0.5MPa) are applied. The red arrow surface is σ_1 and the white arrow surface is σ_3, (a) scoria/ tuff contact, (b) scoria/ lava contact, (c) lava/scoria contact (y-axis in meters).

Table 1: Modelling results for dyke 1 with an applied overpressure (P_o) of 1MPa and an additional horizontal extension of 0.5 MPa. The table also includes a qualitative interpretation of the dyke propagation path as defined through numerical modelling. Tensile stress is measured directly ahead of the dyke tip (Low: 0.5- 1.5MPa, Moderate: 1.5-3MPa, High: 3-5MPa). The condition for propagation is met if the stress at the tip exceeds 0.5 MPa and if the trajectory of σ_1 is close to 90˚. The dyke propagates in a σ_1 and σ_3 plane and their trajectories are shown in the models. The intermediate principal stress (σ_2) was calculated (if possible) from numerical models not shown here.

(A1) P_o= 1MPa	**Layer contacts (E_U/E_L)**	**Stress concentration at the tip**	**Stress rotation at the tip and its vicinity**	**Dyke path**	**(B1) P_o=1MPa and 0.5 MPa extension**	**Stress concentration at the tip**	**Stress rotation at the tip and its vicinity**	**Dyke path**
(a)	Scoria/ Tuff	Low	(σ_1): 0˚- 45˚ (σ_2): N/A (σ_3): 0˚- 45˚ (A1-a)	Propagation	**(a)**	Low	(σ_1): 0˚- 45˚ (σ_2): 0˚- 45˚ (σ_3): 0˚- 45˚ (B1-a)	Propagation
(b)	Scoria/ Lava	Moderate	(σ_1): 0˚- 45˚ (σ_2): 0˚- 45˚ (σ_3): 0˚- 45˚ (A1-b)	Propagation	**(b)**	Moderate	(σ_1): 0˚- 45˚ (σ_2): 0˚- 45˚ (σ_3): 0˚- 45˚ (B1-b)	Propagation
(c)	Lava/ Scoria	Moderate	(σ_1): 0˚- 10˚ (σ_2): N/A (σ_3): 0˚- 10˚ (A1-c)	Propagation	**(c)**	Moderate	(σ_1): 0˚- 10˚ (σ_2): 0˚- 10˚ (σ_3): 0˚- 10˚ (B1-c)	Propagation

6.2.2 Dyke 1 with a 5 MPa driving pressure

Here we modelled dyke 1 by changing the overpressure (P_o) to 5MPa. The models are shown in Fig. 10 and the results in Table 2. We find that dyke tip tensional stresses concentrate both in the tuff layer (E2) and in the scoria (E3) layer, although we note that there is much greater concentration of tensile stress in the lava (E4) unit. The trajectories of σ_1 are generally vertical indicating that the propagation dyke path in this model would favour vertical propagation. In model A2-b the tensional stress concentrates within the lava flow (E4) and less in the overlying scoria (E5) layer. However, the trajectories of σ_1 are oriented sub-vertically directly above the dyke tip which suggests a sub-vertical path if the dyke were to continue propagating. In the vicinity of the dyke tip, the trajectories of σ_1 and σ_3 dip from 0° to 45° within a few tens of cm up to the next contact between scoria (E5) and the lava (E6). In the following model (A2-c) the σ_1 - σ_3 plane rotates by 10°.

The application of a 0.5 MPa horizontal extension in this suite of models (B2a-c) creates similar results and stress rotations as in A2a-c although the σ_1 plane rotates by 10°. These stress conditions all encourage dyke propagation.

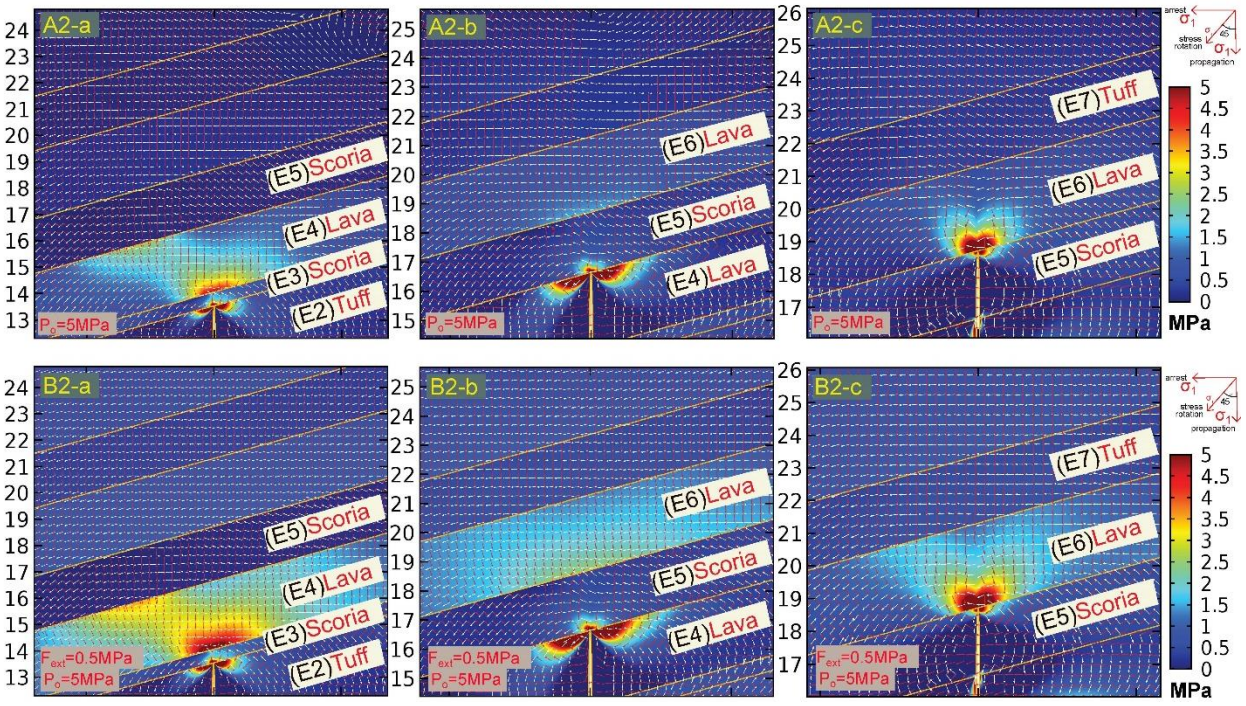

Figure 10: FEM (finite element) models of dyke propagation (tensile stress σ_3) in a heterogeneous host rock based on Fig. 8B. (A2a-c): Overpressure (P_o=5MPa) is the only loading boundary

condition, (B2a-c): Overpressure (P_o=5MPa) and an extensional stress field (F_{ext}=0.5MPa) are applied. The red arrow surface is σ_1 and the white arrow surface is σ_3, (a) scoria/ tuff contact, (b) scoria/ lava contact, (c) lava/scoria contact (y-axis in meters).

Table 2: Modelling results for dyke 1 with an applied overpressure (P_o) of 5MPa and an additional horizontal extension of 0.5 MPa. The table also includes a qualitative interpretation of the dyke propagation path as defined through numerical modelling. Tensile stress is measured directly in ahead of the dyke tip (Low: 0.5- 1.5MPa, Moderate: 1.5-3MPa, High: 3-5MPa). The condition for propagation is met if the stress at the tip exceeds 0.5 MPa and if the trajectory of σ_1 is close to 90˚. The dyke propagates in a σ_1 and σ_3 plane and their trajectories are shown in the models. The intermediate principal stress (σ_2) was calculated (if possible) from numerical models not shown here.

(A2) P_o=5 MPa	**Layer contacts (E_U/E_L)**	**Stress concentration at the tip**	**Stress rotation at the tip and its vicinity**	**Dyke path**	**(B2) P_o=5MPa and 0.5 MPa extension**	**Stress concentration at the tip**	**Stress rotation at the tip and its vicinity**	**Dyke path**
(a)	Scoria/ Tuff	High	(σ_1): 0˚- 10˚ (σ_2): N/A (σ_3): 0˚- 10˚ (A2-a)	Propagation	**(a)**	Low	(σ_1): 0˚- 10˚ (σ_2): 0˚- 45˚ (σ_3): 0˚- 10˚ (B2-a)	Propagation
(b)	Scoria/ Lava	High	(σ_1): 0˚- 45˚ (σ_2): 0˚- 45˚ (σ_3): 0˚- 45˚ (A2-b)	Propagation	**(b)**	High	(σ_1): 0˚- 45˚ (σ_2): 0˚- 45˚ (σ_3): 0˚- 45˚ (B2-b)	Propagation
(c)	Lava/ Scoria	High	(σ_1): 0˚- 10˚ (σ_2): 0˚- 45˚ (σ_3): 0˚- 10˚ (A2-c)	Propagation	**(c)**	High	(σ_1): 0˚- 10˚ (σ_2): 0˚- 10˚ (σ_3): 0˚- 10˚ (B2-c)	Propagation

6.3 Dyke 2

Dyke 2 is an arrested mafic dyke but otherwise very similar to dyke 1 (Fig. 11A). The host rock again is composed of six layers of dissimilar mechanical materials while their thicknesses and sequence differ from those in the previous models. We again produce 2D snapshots of the dyke stresses very close to the same three mechanically different contacts (which are those seen in the field at different depths) and for the two loading boundary conditions. The three contacts denoted with a star are as follows (Fig. 11B):

Contact 1: scoria (E3 = 0.5 GPa) - tuff (E2 = 5 GPa) –/ very compliant-compliant, E=0.5/5, (r=0.1)

Contact 2: scoria (E5 = 0.5 GPa) - lava (E4 = 10 GPa) –/ very compliant-stiff, E=0.5/10, (r=0.05)

Contact 3: lava (E6 = 10 GPa) - scoria (E5 = 0.5 GPa) –/ stiff- very compliant, E=10/0.5, (r=20)

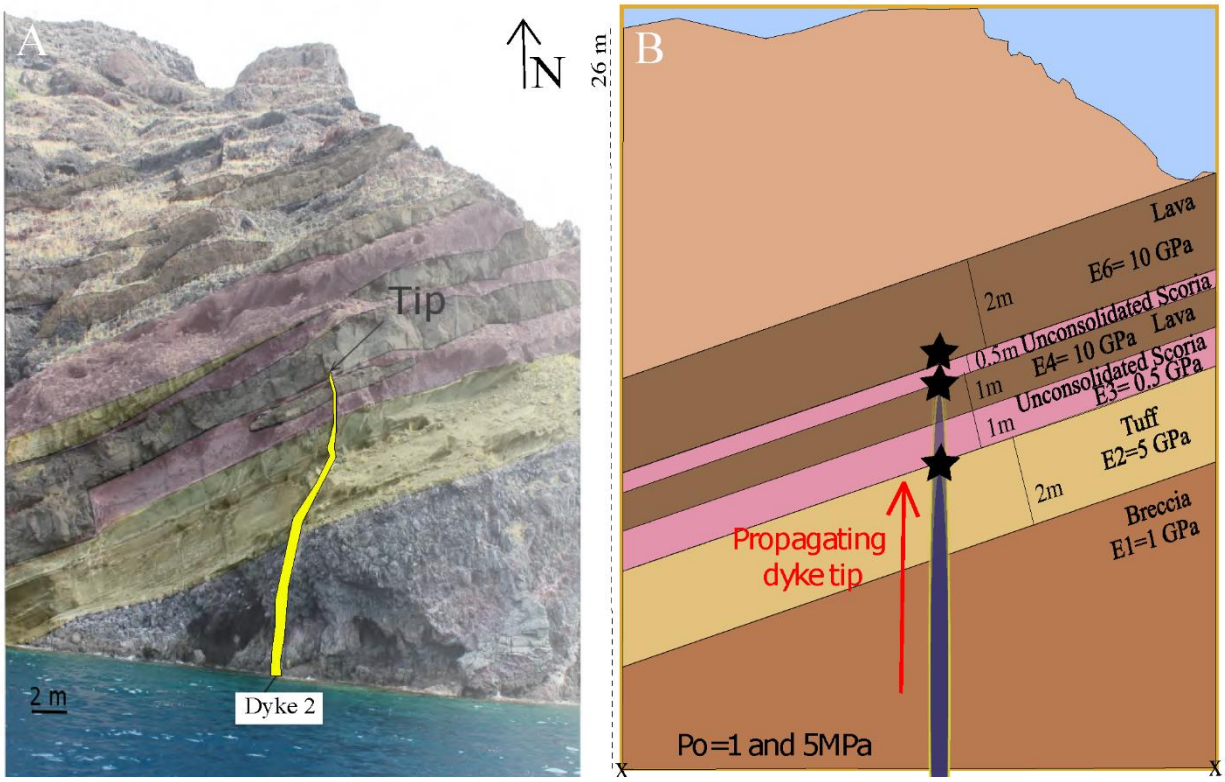

Figure 11: Dyke 2 has thinned out and became arrested within a lava unit in the northern caldera wall. (A): annotated field photograph, (B): FEM model setup. The stars correspond to the specific picked contacts from which 2D snapshots were produced in COMSOL Multiphysics as the dyke is propagating towards the surface.

6.3.1 Dyke 2 with a 1 MPa overpressure

We initially modelled dyke 2 with a 1 MPa driving pressure (P_o) (A3a-c) and then added an additional regional extension of 0.5 MPa (B3a-c). The models are shown in Fig. 12 and the results in Table 3. In model A3-a the dyke tip tensional stresses are concentrated predominantly in the tuff (E2) and lava (E4) and less so in the scoria (E3) layer. The trajectories of the maximum principal compressive stress (σ_1) in front of the tip are oriented along the dyke flow. There is also stress concentrations at the scoria (E5) and lava (E6) contact in conjunction with σ_1 stress rotation of almost 90°. In model A3-b the tensional stress is concentrated within the lava layer (E4) and only slightly in the overlying scoria (E5) unit. However, the trajectories of σ_1 rotated by approximately 45° directly above the dyke tip and close to 90° in the overlying scoria (E5) and lava (E6) contact which would likely favour arrest. In the next set of unit contacts (A3-c) the tensional stresses are concentrated above the dyke tip in the stiff lava (E6) unit, and the stress trajectories are both nearly vertical.

Accordingly, in model B3-a and B3-b,the dyke tip tensional stresses and the trajectories of σ_1 follow similar patterns with A3-a and A3-b. Also, in the next set of unit contacts (B3-c), the tensile stresses are concentrated above the dyke tip in the stiff lava (E6), and σ_1 is vertical which indicates a high likelihood of propagation like A3-c.

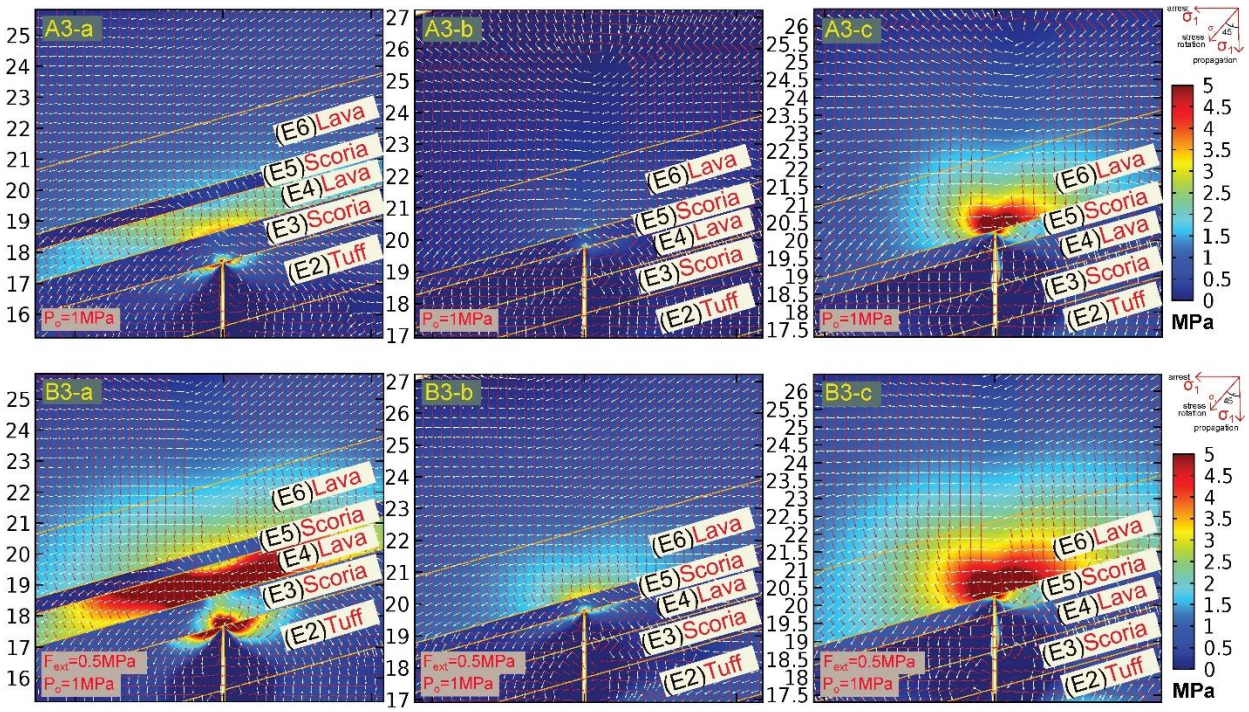

Figure 12: FEM (finite element) models of dyke propagation (tensile stress σ_3) in a heterogeneous host rock based on Fig. 11B. (A3a-c): Overpressure (P_o=1MPa) is the only loading boundary condition, (B3a-c): Overpressure (P_o=1MPa) and an extensional stress field (F_{ext}=0.5MPa) are applied. The red arrow surface is σ_1 and the white arrow surface is σ_3, (a) scoria/tuff contact, (b) scoria/lava contact, (c) lava/scoria contact (y-axis in meters).

Table 3: Modelling results for dyke 2 with an applied overpressure (P_o) of 1MPa and an additional horizontal extension of 0.5 MPa. The table also includes a qualitative interpretation of the dyke propagation path as defined through numerical modelling. Tensile stress is measured directly in ahead of the dyke tip (Low: 0.5- 1.5MPa, Moderate: 1.5-3MPa, High: 3-5MPa). The condition for propagation is met if the stress at the tip exceeds 0.5 MPa and if the trajectory of σ_1 is close to 90˚. The dyke propagates in a σ_1 and σ_3 plane and their trajectories are shown in the models. The intermediate principal stress (σ_2) was calculated (if possible) from numerical models not shown here.

(A3) P_o=1 MPa	**Layer contacts (E_U/E_L)**	**Stress concentration at the tip**	**Stress rotation at the tip and its vicinity**	**Dyke path**	**(B3) P_o=1MPa and 0.5 MPa extension**	**Stress concentration at the tip**	**Stress rotation at the tip and its vicinity**	**Dyke path**
(a)	Scoria/Tuff	Moderate	(σ_1): 0˚- 90˚ (σ_2): 0˚- 90˚ (σ_3): 0˚- 90˚ (A3-a)	Likely Arrest	**(a)**	High	(σ_1): 0˚- 90˚ (σ_2): 0˚- 90˚ (σ_3): 0˚- 90˚ (B3-a)	Likely Arrest
(b)	Scoria/Lava	Moderate	(σ_1): 0˚- 90˚ (σ_2): 0˚- 90˚ (σ_3): 0˚- 90˚ (A3-b)	Likely Arrest	**(b)**	Moderate	(σ_1): 0˚- 90˚ (σ_2): 0˚- 90˚ (σ_3): 0˚- 90˚ (B3-b)	Likely Arrest
(c)	Lava/Scoria	Low	(σ_1): 0˚- 10˚ (σ_2): 0˚- 10˚ (σ_3): 0˚- 10˚ (A3-c)	Propagation	**(c)**	High	(σ_1): 0˚- 10˚ (σ_2): 0˚- 10˚ (σ_3): 0˚- 10˚ (B3-c)	Propagation

6.3.2 Dyke 2 with a 5 MPa driving pressure

We modelled dyke 2 by modifying only the overpressure (P_o) to 5MPa. The models are shown in Fig. 13 and the results in Table 4.

The results from models A4-a and A4-b are similar to models A3-a and A3-b and show a higher concentration of stresses at the same locations and within the same rock units. The trajectories of σ_1 rotate by approximately at 45° directly above the dyke tip and up to 90° at the overlying scoria (E5) and lava (E6) contact promoting possible arrest - although the scoria (E5) and lava (E6) contact (A4-c) indicates no stress rotations. Models B4-a-c were developed similarly and also suggest the likelihood of dyke arrest at the scoria (E5) and lava (E6) contact.

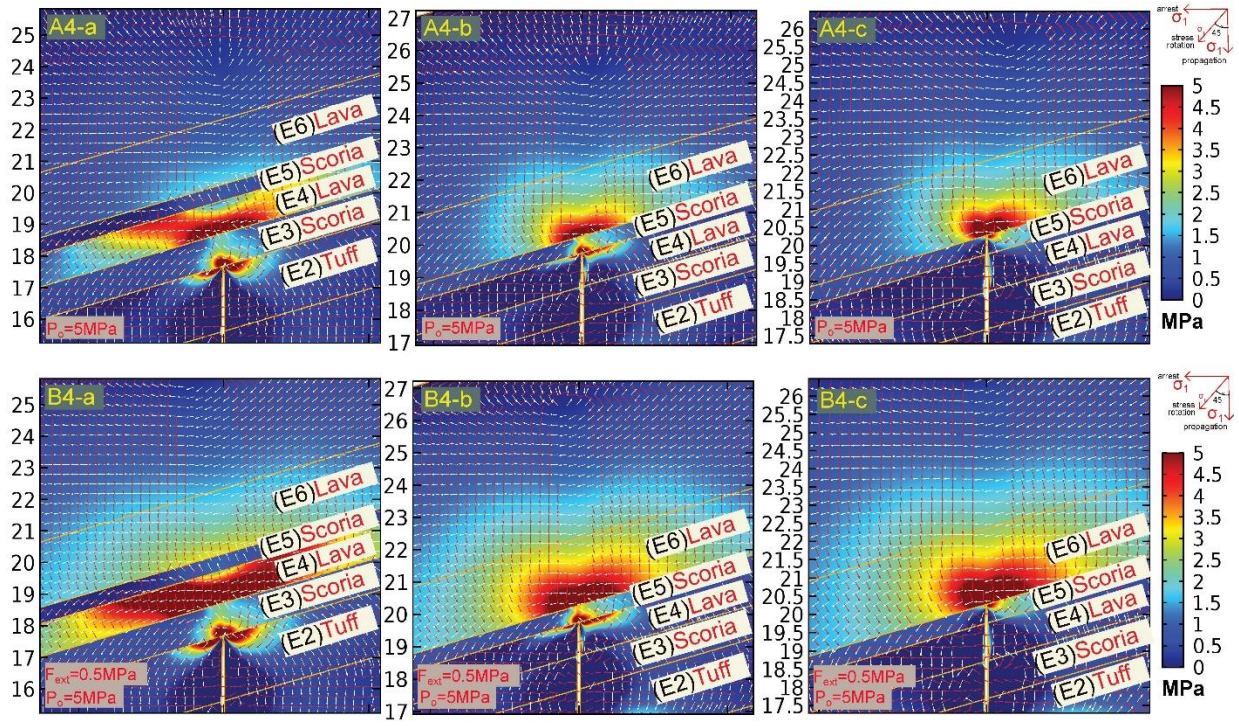

Figure 13: FEM (finite element) models of dyke propagation (tensile stress σ_3) in a heterogeneous host rock based on Fig. 11B. (A4a-c): Overpressure (P_o=5MPa) is the only loading boundary condition, (B4a-c): Overpressure (P_o=5MPa) and an extensional stress field (F_{ext}=0.5MPa) are applied. The red arrow surface is σ_1 and the white arrow surface is σ_3, (a) scoria/tuff contact, (b) scoria/lava contact, (c) lava/scoria contact (y-axis in meters).

Table 4: Modelling results for dyke 2 with an applied overpressure (P_o) of 5MPa and an additional horizontal extension of 0.5 MPa. The table also includes a qualitative interpretation of the dyke propagation path as defined through numerical modelling. Tensile stress is measured directly in ahead of the dyke tip (Low: 0.5- 1.5MPa, Moderate: 1.5-3MPa, High: 3-5MPa). The condition for propagation is met if the stress at the tip exceeds 0.5 MPa and if the trajectory of σ_1 is close to 90˚. The dyke propagates in a σ_1 and σ_3 plane and their trajectories are shown in the models. The intermediate principal stress (σ_2) was calculated (if possible) from numerical models not shown here.

(A4) P_o=5 MPa	**Layer contacts (E_U/E_L)**	**Stress concentration at the tip**	**Stress rotation at the tip and its vicinity**	**Dyke path**	**(B4) P_o=5MPa and 0.5 MPa extension**	**Stress concentration at the tip**	**Stress rotation at the tip and its vicinity**	**Dyke path**
(a)	Scoria/Tuff	High	(σ_1): 0˚- 90˚ (σ_2): 0˚- 90˚ (σ_3): 0˚- 90˚ (A4-a)	Likely Arrest	**(a)**	High	(σ_1): 0˚- 90˚ (σ_2): 0˚- 90˚ (σ_3): 0˚- 90˚ (B4-a)	Likely Arrest
(b)	Scoria/Lava	High	(σ_1): 0˚- 90˚ (σ_2): 0˚- 90˚ (σ_3): 0˚- 90˚ (A4-b)	Likely Arrest	**(b)**	High	(σ_1): 0˚- 90˚ (σ_2): 0˚- 90˚ (σ_3): 0˚- 90˚ (B4-b)	Likely Arrest
(c)	Lava/Scoria	High	(σ_1): 0˚- 10˚ (σ_2): 0˚- 10˚ (σ_3): 0˚- 10˚ (A4-c)	Propagation	**(c)**	High	(σ_1): 0˚- 10˚ (σ_2): 0˚- 10˚ (σ_3): 0˚- 10˚ (B4-c)	Propagation

6.4 Theoretical stress concentration at the dyke tips

For dyke 1 we report a range of theoretical stresses at the dyke tips. For 1MPa magmatic overpressure the maximum theoretical stress concentrating at the tip of the dyke at a 1) very compliant-compliant contact is 0.23 GPa, 2) very compliant-stiff contact is 2.28 GPa, 3) stiff-very compliant contact is 0.13 GPa. For an extra horizontal extension, the stress at the tips rises in the first contact by 40%, in the second by 78% and in the third by 62% generating maximum stresses of 0.32 GPa, 4.05 GPa and 0.2 GPa respectively. For 5 MPa overpressure, the calculated maximum stress is 1.1 GPa for the first contact (r=0.1), 11.4 GPa for the second contact (r=0.05) and 0.67 GPa for the third (r=20) and by adding the extra horizontal extension the stresses increase to 1.43 GPa (30%), 13.2 GPa (16%) and 0.75 GPa (12%).

We used the same methodology for dyke 2 and calculated the maximum stress concentration for 1 MPa magmatic overpressure in the same three contacts which showed 0.22 GPa, 0.67 GPa and 0.10 GPa. For an extra horizontal extension, the stress at the tips rises in the first contact by 68%, in the second by 70% and in the third one by 80% presenting maximum stresses of 0.37 GPa, 1.14 GPa and 0.18 GPa respectively. For 5 MPa the calculated maximum stress is 1.13 GPa for the first contact (r=0.1), 3.82 GPa for the second contact (r=0.05) and 0.61 GPa for the third one (r=20) and they rise to 1.43 GPa (13%), 13.2 GPa (14%) and 0.75 GPa (16%). The results are shown in Fig. 14.

All these tip stresses are entirely theoretical and follow primarily from the mechanical properties of the layers hosting the tips and, in particular, from the geometric constraints (tips are commonly very narrow), and the applied load (overpressure). The stress magnitudes are similar to those obtained for dyke tips in other numerical models (Gudmundsson, 2003). For comparison, analytical mathematical mode I crack models yield infinite stresses (a singularity) at the tip (Sneddon, 1946). No rocks are known to tolerate in-situ tensile stresses in excess of about 9 MPa (Gudmundsson, 2011b).

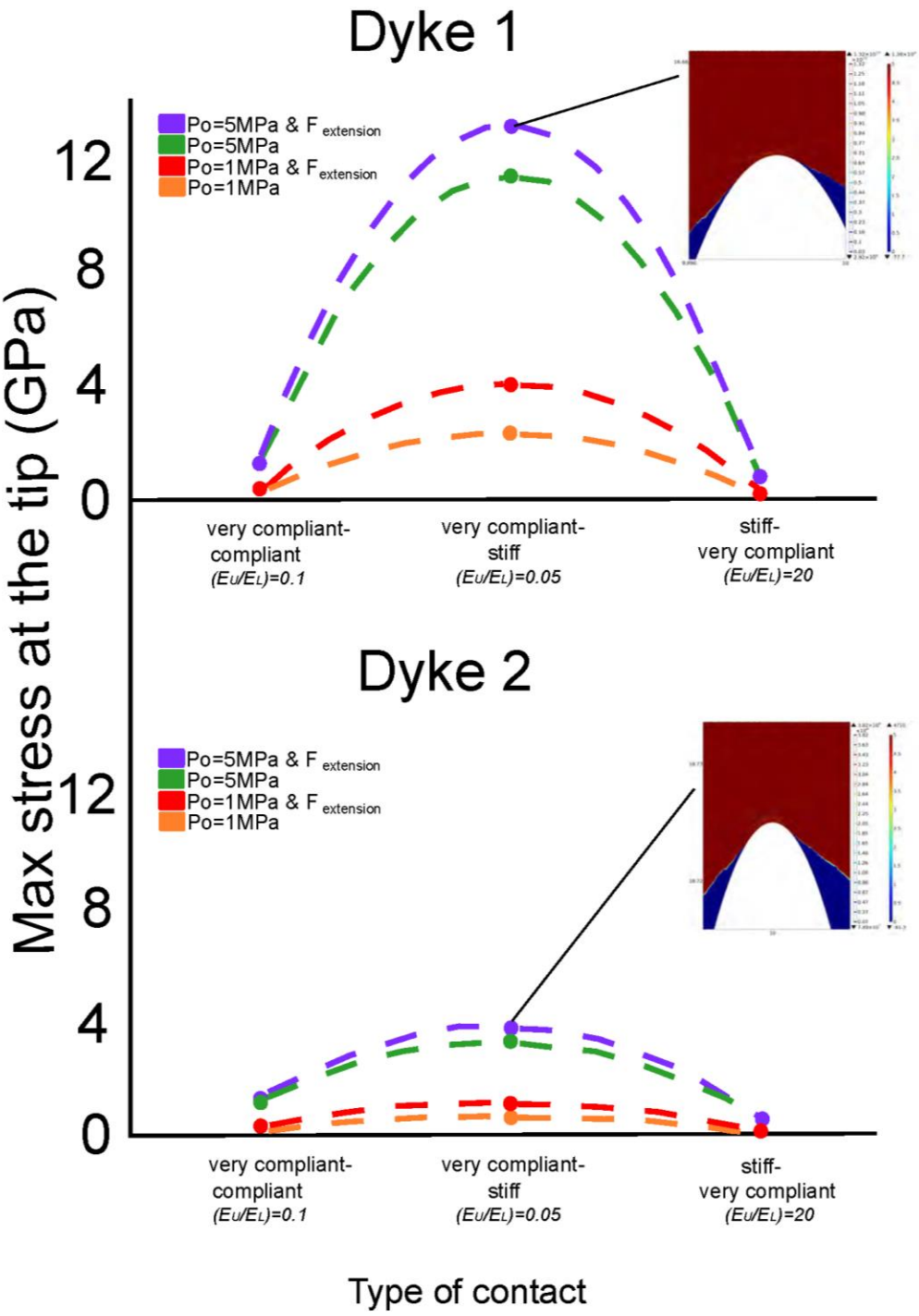

Figure 14: Diagram showing the max stress concentration at the dyke tips for both dykes at the studied loading conditions, in different type of contacts 1) very compliant - compliant (r=0.1), 2) very compliant - stiff (r=0.05), 3) stiff - very compliant (r=20). The figures on the right up corner of the graphs are showing the stress concentration on the dyke tips at the compliant - stiff contacts for dyke 1 and dyke 2.

6.5 Sensitivity tests

Although the numerical models agree with the field observations indicating that stress rotations contributed to the arrest of dyke 2, the questions as to which factors encourage stress rotations and subsequently the formation of stress barriers, are only partially answered. For that reason, we conducted multiple runs (sensitivity tests) to explore the possible cause(s) that could promote stress rotations at the tip of dyke 2.

We investigated the contribution of combinations of parameters in our numerical model setups. Two suites of sensitivity tests were designed to reflect the possible arrest conditions. Initially, the study focused on the combination of the material and magmatic properties (Fig. 15A), and in a second stage, we studied the external stress field with the material properties of the host rock (Fig. 15B). The sensitivity test models are shown in the supplementary files (Supporting information files 1-6).

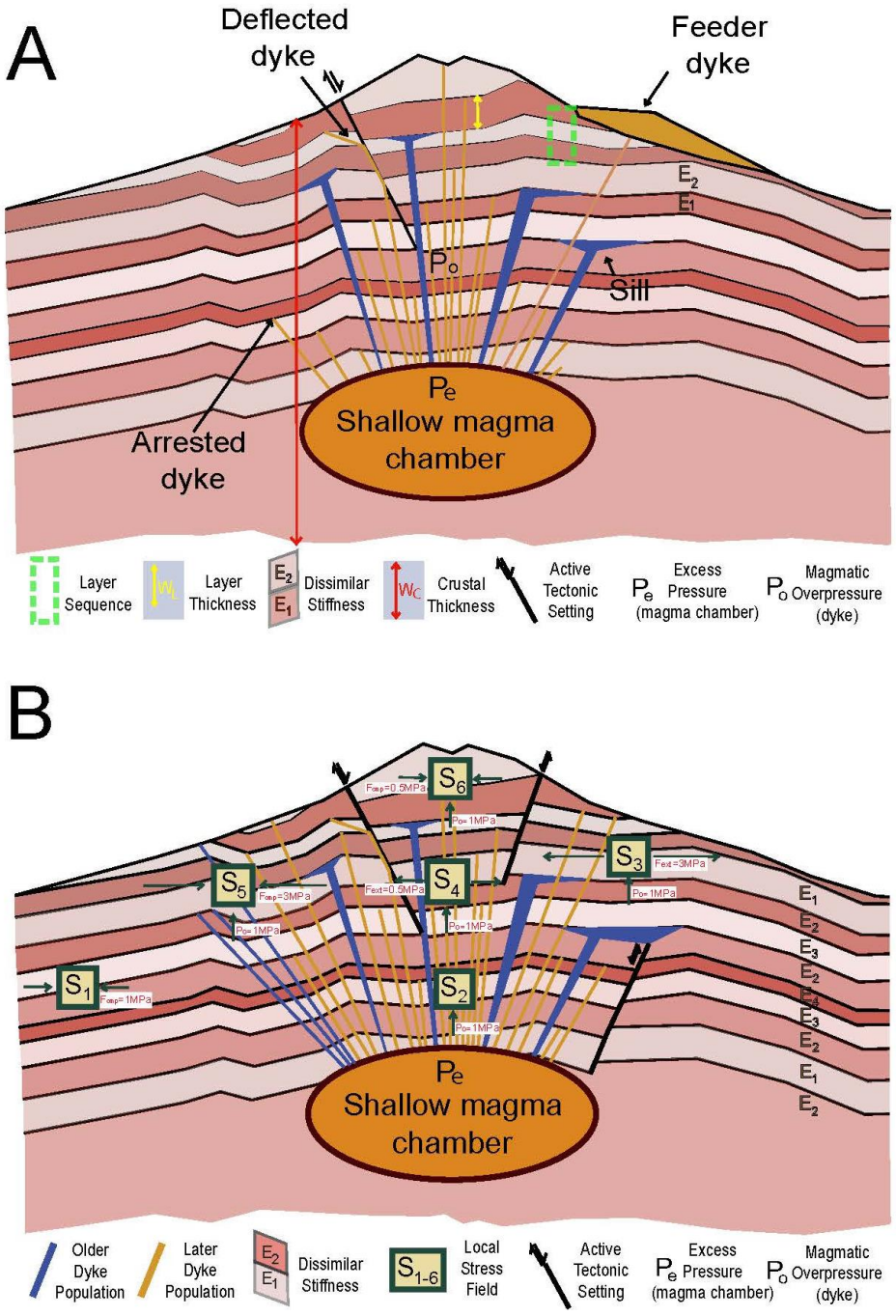

Figure 15: Schematic illustrations showing the parameters studied in the sensitivity tests. (A): Connections between magmatic conditions (magmatic overpressure, P_o) and the stratigraphy-mechanical/material conditions of the host rock such as the sequence of the stratigraphy, the thickness of the layers (W_L), and the crustal thickness (W_C). (B): Conditions of magmatic overpressure (P_o) associated with different boundary conditions on the creation of stress rotations and stress barriers in an active volcanotectonic setting.

Layer thickness (W_L):

We modelled the effects of layer thickness on the local stress and found that principal-stress rotations were mostly controlled by the stiffness contrast of the layers. However, when the thickness of a stiff layer (e.g. a lava flow) is increased by a factor of ten we observe stress rotations in the lava layer and in the vicinity of the dyke tip regardless the stiffness values (Fig. 16-1). In addition, when the thickness of a soft layer (e.g. scoria) is increased by a factor of ten, stress rotations in both the scoria and lava layers were observed in the vicinity of the dyke tip at a low stiffness contrast (Fig. 16-2). Thus, a thick stiff layer can become a stress barrier whereas a thick soft layer can generate stress rotations if the dyke propagates through soft layers with low stiffness contrasts (r=0.5)

Stratigraphic sequence

The sensitivity models reflect how effectively the stratigraphy of the host rock together with the stiffness of the layers can control stress rotations. Stress rotations were observed only when the stiffness contrast was low (r=0.5 or 5). Apparently, this parameter can make soft layers to stress barriers as shown in Figure16-3.

Crustal thickness (Wc)

We tested how the variable thickness of the crust can promote stress rotations. In our models as shown in Figure 16-4 we designed thicker domains by adding an extra thick layer atop the sequence. We observed that a thick sequence can generate stress rotations especially in compliant layers such as scoria if the dyke propagates again through layers of high stiffness contrast (r=50).

Overpressure (P_o):

We made many models to test the effect of overpressure on dyke arrest. The magmatic overpressure is important parameter as it provides to the dyke the essential pressure to propagate subject to a satisfactory energy criterion. However, other parameters are also important in that they control principal stress rotation and other effects that lead to dyke arrest. We did not test the

relation between the overpressure and dyke thickness because both studied dykes are of the same average thickness. We know, however, that the aperture or thickness of the dyke is positively correlated with its overpressure (Eq.6).

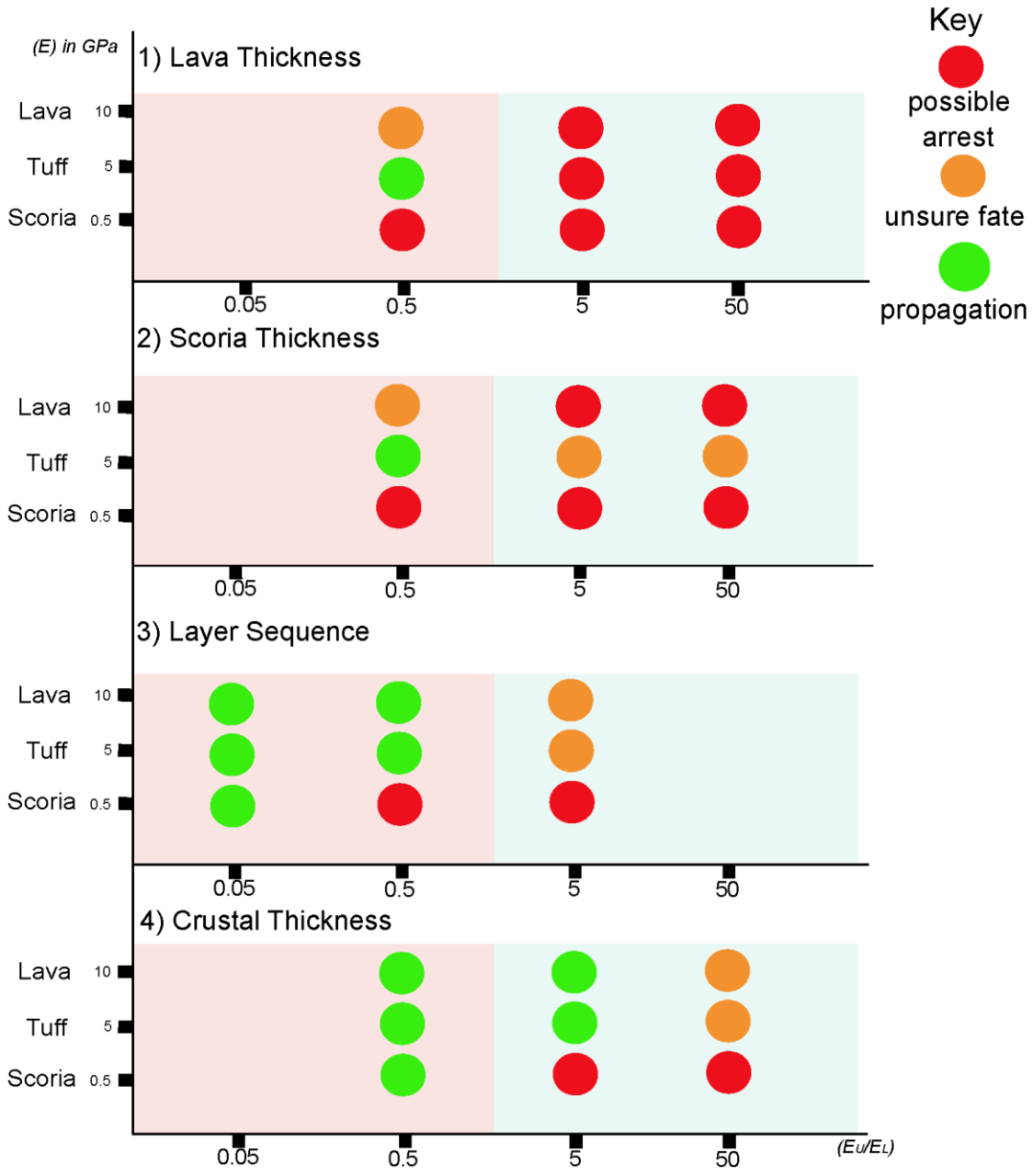

Figure 16: Results of the sensitivity tests as shown in Fig. 15 Part A. Different stiffness contrasts (E_U/E_L) (0.05, 0.5, 5, 50) subject to 1 and 5MPa overpressure control the observed stress rotations in three different rock type layers. Annotations: Red circle for possibly arrest, orange for unsure fate and green for propagation.

Regional and local stress field

We examined stress rotations under different loading boundary conditions and with layers of contrasting stiffness (Fig. 17). The S1 scenario was used as a benchmark model while S2 mainly describes the conditions close to a magma chamber where the overpressure should be sufficient as a principal control on the propagation of the dyke. The scenarios S3&4 simulate an extensional regime such as a rift zone, or the regional extension due to the extension and the rapid roll-back that the Aegean Sea experiences. The models clearly show that if a dyke propagates in an extensional stress regime (Fig. 17-S3&4) stress rotation can occur in all layers for every studied stiffness contrast except in compliant layers (e.g. scoria) when a dyke propagates from a soft/compliant to a stiff layer (r=50). However, under a horizontal compression (Fig. 17-S5&6) stress rotations can occur again regardless of the stiffness contrasts in all type of layers except in a soft layer (e.g. scoria) where propagation can be encouraged in high stiffness contrasts (r=50). Compressional stress fields describe regional stress conditions due to previous dyke injections, faulting, or graben subsidence.

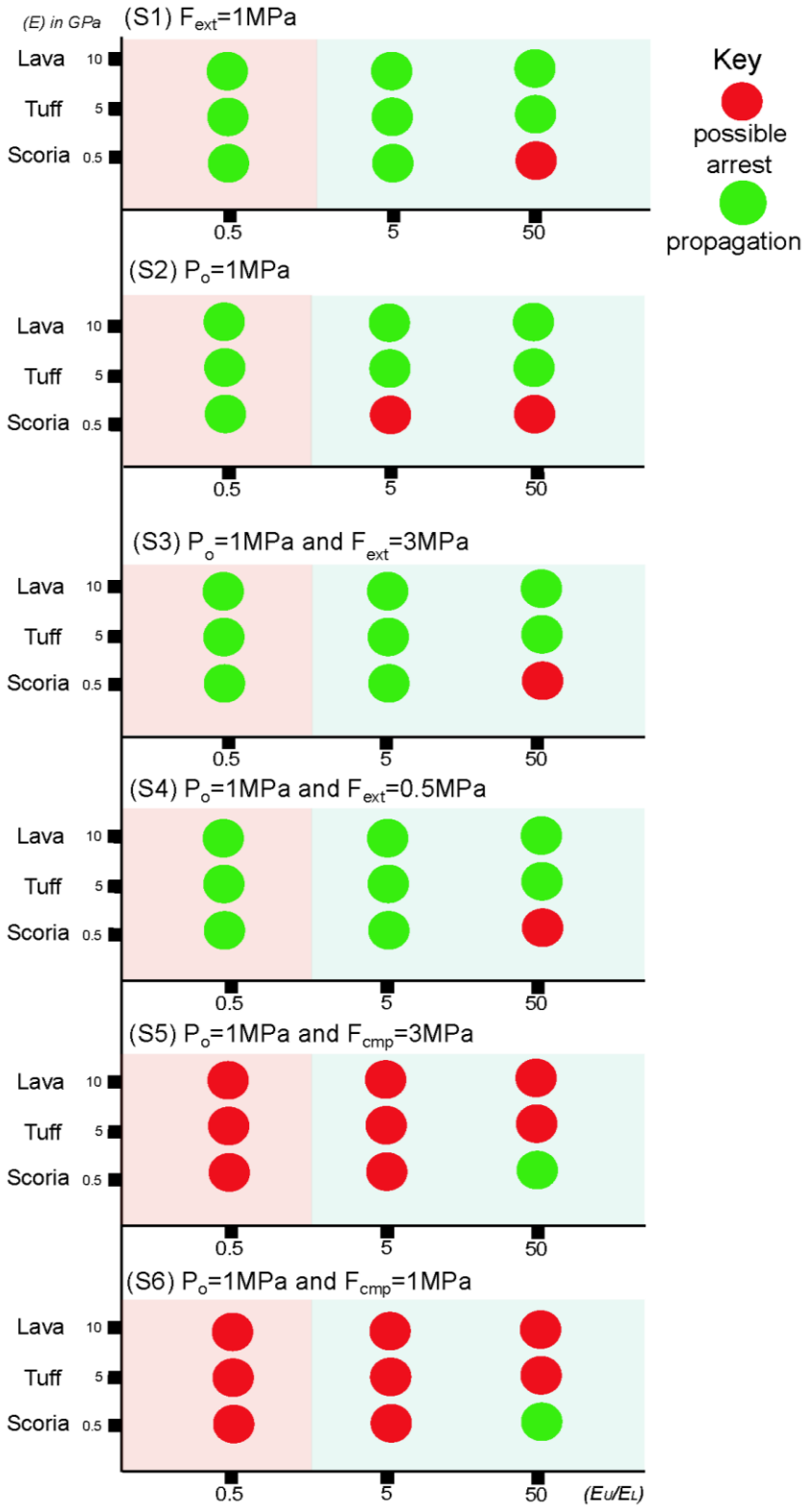
(E) in GPa
(S1) F_ext=1MPa
Lava 10
Tuff 5
Scoria 0.5
0.5
5
50
Key
possible arrest
propagation
(S2) P_o=1MPa
(S3) P_o=1MPa and F_ext=3MPa
(S4) P_o=1MPa and F_ext=0.5MPa
(S5) P_o=1MPa and F_cmp=3MPa
(S6) P_o=1MPa and F_cmp=1MPa
(Eu/EL)

Figure 17: Figure showing the results of the second model suites of the sensitivity tests as shown in Fig. 15 Part B subject to different stiffness contrasts (E_U/E_L) (0.5, 5, 50). We observe the mutual connections between the magmatic conditions subjected to changes in the local stress field and producing stress barriers. S1: application of horizontal extension (F_{ext}= 1MPa), S2: application of magmatic overpressure (P_o=1MPa), S3: application of magmatic overpressure (P_o=1MPa) and horizontal extension (F_{ext}= 3MPa), S4: application of magmatic overpressure (P_o=1MPa) and horizontal extension (F_{ext}= 0.5MPa), S5: application of magmatic overpressure (P_o=1MPa) and horizontal compression (F_{cmp}= 3MPa), S6: application of magmatic overpressure (P_o=1MPa) and horizontal compression (F_{cmp}= 0.5MPa).

7. Discussion

The results of the numerical models have various theoretical and applied implications. For example, we calculated the theoretical tensile stresses ahead of a dyke snapshot in both homogeneous and heterogeneous crustal segments. We found that the tensile stress increases with increasing overpressure as well as with horizontal extension at the model boundary (Figs. 9-10 and 12-13). In addition, higher stresses concentrate in the stiff lava layers while the soft scoria and tuff layers suppress the stresses.

We also investigated the theoretical stresses close to and at the tips in all the studied types of contacts (Fig. 14). The results show that the tensile stresses at the tip can theoretically become 3 to 4 orders of magnitude higher than the overpressure. In detail, the study revealed the following for both the dykes:

1) Stress concentration is positively correlated with the stiffness of the host rock layers. More specifically, the stiffer they are, the higher the theoretical tensile stress.
2) Stress concentration is also positively correlated with magmatic overpressure and with the application of the external horizontal extension. More specifically, when either of these increases, then so does the theoretical tensile stress.

The numerical models also show that crustal anisotropy (layering) has a substantial effect on the alignment and rotation of principal stresses. This is of great importance for dyke paths and the

potential for eruption. For example, rotation of σ_1 from being vertical to horizontal will almost always result in the arrest - or deflection into a sill - of a vertically propagating dyke, the layer with the rotated stresses acting as a stress barrier.

However, a stress barrier was not generated in any of the models for dyke 1. As a result, the numerical modelling supports the field-based indication of a continuous and non-arrested path, albeit with slight variations in path dip. In the models for dyke 2, we observed minor stress rotations at the contact between the tuff and unconsolidated scoria (as shown in part A3a-c of Fig. 12). By contrast, stress rotations of up to 90° were observed at the contact between very stiff lava flows and soft layers such as unconsolidated scoria (as shown in part B3-a of Fig. 12), generating stress barriers. The dyke in this instance, however, may also have become arrested by the elastic mismatch process as the soft unconsolidated scoria and the stiff lava flows have very different elastic properties (Young's modulus). This is very much in agreement with the field observations which clearly show that the dyke tip thinned out gradually until it stopped at the E6 (lava) - E5 (scoria) contact.

We also made comparisons of the present results with laboratory experiments. Analogue models (Kavanagh et al., 2006) suggest that a dyke may become arrested when the driving pressure is almost equal to the excess pressure needed for a dyke to penetrate the stiffer layer atop. We compared the proposed dyke paths (with possible stress rotations) of our tested stiffness ratios with the proposed experimental dimensionless stiffness ratios (two-layered system with high stiffness ratios) from Kavanagh et al., (2006). The results showed that experimentally arrested dykes form when the ratio of E_U/E_L is 14.95. In our models with a six-layer sequence, Eq. 6 indicates that dyke 2 would promote stress rotations and become arrested when the ratio of E_U/E_L was as high as 20 (E_U/E_L=10/0.5=20) and so in agreement with the analogue experiments.

2D BEM numerical models and laboratory experiments (Maccaferri et al., 2010) suggest that the elastic energy release rate (G) during crack propagation through a boundary from a soft to a stiff layered elastic body with high stiffness contrast diminishes steeply promoting dyke deflection to inclined sheets. These results are in agreement with analytical results on the effects of elastic mismatch on mode I fracture deflection (He and Hutchinson, 1989; Gudmundsson, 2011a,b). Our models show that vertical dykes with the same stiffness contrast (r=5 or 20) can produce stress

rotations and probably dyke arrest in heterogeneous domains. Future studies on how the energy criteria affect the dyke propagation paths in terms of their dip should be encouraged.

The numerical models indicate that dyke arrest can occur due to variations in mechanical properties of layers, particularly in stiffness (Young's modulus). Layer stiffness, however, changes during time and depends on the age of and depth below the surface at the time of dyke emplacement. Generally, rock layers become stiffer with time, particularly pyroclastic and sedimentary layers, primarily due to secondary mineralisation and compaction. Thus, generally, the tendency to dyke arrest is greatest in a comparatively young stratovolcano while the mechanical contrast between layers that constitute the roof of the source chamber is great. Gradually, due to compaction and mineralisation, the mechanical properties of the crustal segments or sequences become more similar, that is, homogenized, and normally easier to penetrate by dykes. Thus, contacts that early in the history of the volcano arrest dykes, may allow dykes to penetrate later in the history of the volcano.

This brings us to the age of the layers and thus to a brief overview of the relevant geological history of the sections dissected by dykes 1 and 2. The deposition of av1 (Fig. 4) took place between 530-430 ka followed by av2 and av3 horizons which formed the Peristeria stratovolcano. Later eruptions formed the cinder cones and then the Skaros and Therasia shields on top of the stratigraphy of Peristeria. The oldest dyke population in Figure 4, which strikes NW-SE was possibly emplaced during the formation of the Peristeria volcano as it was found to dissect only the av1 horizon. The dykes are extensively weathered and of a characteristic red (or light) colour possibly due to oxidation and are likely of felsic composition. A second, younger dyke population was emplaced in the same section, cross-cutting the stratigraphy and the earlier dykes. These dykes strike NE-SW and have an average thickness of 0.5 m and are generally of mafic composition. Dyke 1 propagated to the higher stratigraphic horizons while dyke 2 became arrested at the contact between a scoria and a lava layer in av1.

The host rock is formed by a seemingly random sequence of andesitic lavas, tuffs, scoria and breccia (hyaloclastites). The layers are dipping 20° to the east and have variable thicknesses. The base layer is formed by a sequence of lava and breccia with variable thickness and grain size.

Given the structural study of the area, the possible scenarios of the observed dyke path are:

1) Dyke 1 and dyke 2 were emplaced after the formation of the Peristeria volcano. The emplacement of dyke 1 (or dyke 2) and the paths were then primarily determined by the variation in mechanical properties and local stresses of the layers.

2) Dyke 1 is propagating through the stratigraphy subject to a local compressional stress field imposed by the previous dyke injections and a regional extensional stress field imposed by the rift zone. Dyke 1 may have propagated partly due to the extensional stress field that do not mainly promote stress rotations in combination with low stiffness contrasts (r=0.5 or 5). Subsequently injected dyke 2 interacts with the local stress field imposed by dyke 1.

In detail, dyke paths in the shallow crust are much affected by the local material properties of the rock layers and by associated local stresses. Local stresses commonly generate stress barriers encouraging dyke arrest. Also, while the overpressure is primarily the driving force of dyke propagation from and near the magma chamber (Gudmundsson, 2003), it is not constant and, particularly for mafic dykes injected from shallow chambers, the overpressure tends to decrease towards the surface – because of negative buoyancy (Eq. 5). Other factors that may contribute to dyke arrest, discussed here, include layer thickness and layer stiffness. Stiffness, particularly rather stiffness contrast across contacts, is the most fundamental parameter as regards dyke arrest. This is not only because stiffness largely controls principal stress rotations and the formation of stress barriers, but also because variation in stiffness between layers is the main contribution to elastic mismatch, which is the major contribution to dyke arrest, particularly in stratovolcanoes such as Santorini.

8. Conclusions

Our combined field and numerical modelling study allow the following conclusions to be drawn on the structure and emplacement of dykes within arc volcanic settings such as at Santorini volcano.

1) Host-rock layering and anisotropy largely controls dyke propagation path and arrest in the shallow crust of Santorini volcano. The arrangement of layers with different stiffnesses

determines the local stress fields within a volcano and hence the attitude and fate of the propagating dykes.

2) The dyke swarm at Santorini was formed over several-episodes. Analysis of the attitude and location of dykes indicates that the swarm fed four distinct localities atop.
3) Most dykes injected from a crustal magma chamber do not make it to the surface to feed an eruption; instead, they become arrested, commonly at contacts between mechanically dissimilar layers.
4) Analytical results suggest that the dykes at Santorini formed and propagated under an overpressure (driving pressure) between 0.1 MPa to 6 MPa (90% of the measurements).
5) We suggest that most arrested dykes were either arrested on meeting stress barriers (where σ_1 has rotated to become horizontal instead of vertical) or on meeting contacts between layers of contrasting stiffness, an elastic mismatch. In agreement with stress barriers and elastic mismatch mechanisms, our FEM models show that soft-stiff contrasts (stiff layer hosting dyke tip below the contact with a soft layer above the contact) may encourage dyke penetrating the contact whereas stiff-soft ones can produce stress barriers and elastic mismatch that encourage dyke arrest.
6) The results suggest that thicker lava or scoria layers are more likely to promote stress rotations and dyke arrest than thin layers with the same mechanical properties. By contrast, magmatic overpressure, although partly controlling stress concentrations at dyke tips, cannot as such induce stress rotations.
7) Soft scoria layers can encourage stress rotations/barriers, even when a dyke propagates from a stiff to a soft layer, unless the stiffness contrast stiff-soft-(E_U/E_L) is low.

Acknowledgements

We thank the editor D. Roman and two anonymous reviewers for comments which helped improve this manuscript. Furthermore, we thank A. Rust and K. Cashman for helpful comments and suggestions which significantly improved an earlier version of the manuscript. We also thank N. Forbes Inskip for discussions about the numerical modelling aspects. KD is grateful for a Kirsty Brown memorial fund which enabled fieldwork in the Aegean. JB gratefully acknowledges support from the projects Fondecyt 11190143 and Fondap-Conicyt 15090013.

REFERENCES

Acocella, V., Neri, M., 2003. What makes flank eruptions? The 2001 Etna eruption and its possible triggering mechanisms. Bull Volcanol. 65, 517-529.

Amadei, B., Stephansson, O., 1997. Rock stress and its measurement. Chapman and Hall, London

Anderson, E.M., 1951. Dynamics of faulting and dyke formation, 2nd edn. Olivier and Boyd, Edinburgh.

Andújar, J., Scaillet, B., Pichavant, M., Druitt, T. H., 2015. Differentiation conditions of a basaltic magma from Santorini, and its bearing on the production of andesite in arc settings, J. Petrol. 56, 765–794.

Babiker, M., Gudmundsson A., 2004. The effects on dykes and faults on groundwater flow in an arid land: the Red Sea Hills, Sudan. J. Hydrol. 297, 256-273

Bailey, J. C., Jensen, E., Hansen, A., Kann, A., Kann, K., 2009. Formation of heterogeneous magmatic series beneath North Santorini, South Aegean island arc, Lithos, 110, 20–36.

Barnett, Z.A., Gudmundsson, A., 2014. Numerical modelling of dykes deflected into sills to form a magma chamber. J. Volcanol. Geother. Res. 281, 1-11.

Becerril, L., Galindo, I., Gudmundsson, A., Morales, J. M., 2013. Depth of origin of magma in eruptions. Sci. Rep., 3, 2762; doi:10.1038/srep02762.

Bell, F.G., 2000. Engineering properties of Soils and Rocks, 4th edn. Blackwell, London.

Brun, J.P., Faccenna, C., Gueydan, F., Sokoutis, D., Philippon, M., Kydonakis, K., Gorini, C., 2017. Effects of slab rollback acceleration on Aegean extension. Bulletin of the Geological Society of Greece. 50, 5-23.

Burchardt, S., 2008. New insights in the mechanics of sill emplacement provided by field observations of the Njardvik Sill, Northeast Iceland. J. Volcanol. Geother. Res. 173, 280-288

Broek, D., 1982. Elementary engineering fracture mechanics, The Hague, The Netherlands Martinus Nijhoff.

Browning, J., Gudmundsson, A., 2015. Caldera faults capture and deflect inclined sheets: an alternative mechanism of ring dike formation. Bull. Volcanol. 77, 1-13

Browning, J., Drymoni K., Gudmundsson A., 2015. Forecasting magma-chamber rupture at Santorini volcano, Greece. Sci. Rep.. 5, 15785; doi: 10.1038/srep15785

Cashman, K.V., 2004. Volatile controls on magma ascent and eruption, in Sparks R.S.J. Hawkesworth C.J. (eds.), The State of the Planet: Frontiers and Challenges in Geophysics: Geophysical Monograph 150: Washington, D.C., American Geophysical Union, p.109–124, doi: 10.1029/150GM10.

Cook, J., Gordon, J.E., 1964. A mechanism for the control of crack propagation in all-brittle systems. Proceedings of the Royal Society, Vol 282, 1364-5021, doi.org/10.1098/rspa.1964.0248.

Dahm, T., 2000. On the shape and velocity of fluid-filled fractures in the Earth. Geophys. J. Int. 142, 181-192

Delaney, P., Pollard, D., Ziony, J., McKee E., 1986. Field relations between dikes and joints: emplacement processes and paleostress analysis J. Geophys. Res., 91, 4920-4938

Druitt, T. H., Francaviglia, V., 1992. Caldera formation on Santorini and the physiography of the islands in the late Bronze Age. Bull. Volcanol. 54, 484–493

Druitt, T.H., Edwards, L., Mellors, R.M., Pyle, D.M., Sparks, R.S.J., Lanphere, M., Davis, M., Barriero, B., 1999. Santorini Volcano. Geological Society Memoir No. 19, 165

Dundurs, J., 1969. Edge-bonded dissimilar orthogonal wedges. Journal of Applied Mechanics, 36, 650-652.

Feuillet, N., 2013. The 2011–2012 unrest at Santorini rift: Stress interaction between active faulting and volcanism, Geophys. Res. Lett., 40, 3532–3537, doi:10.1002/grl.50516.

Forbes Inskip, N.D., Meredith, P.G., Chandler, M.R., Gudmundsson, A., 2018. Fracture properties of Nash Point shale as a function of orientation to bedding, J. Geophys. Res. Vol 123, 10, 8428-8444, doi:10.1029/2018JB015943

Fouqué, F.A., 1879. Santorin et ses éruptions. Masson, Paris, 440 pp.

Freund, L.B, and Suresh, S., 2003. Thin film materials: Stress, defect formation and surface evolution. Cambridge University Press, Cambridge.

Garcia, I.G., 2014. Crack initiation in composites at micro and meso scales: Development and applications of finite fracture mechanics. Ph.D. thesis, Universidad de Sevilla, Spain

Gautneb, H., Gudmundsson, A., Oskarsson, N., 1989. Structure, petrochemistry and evolution of a sheet swarm in an Icelandic central volcano. Geol .Mag. 126, 659–673

Geshi, N., Kusumoto, S., Gudmundsson, A., 2010. Geometric difference between non-feeder and feeder dikes. Geology 38, 195-198

Grasemann, B., Schneider, D.A., Stöckli, D. F., Iglseder, C., 2012. Miocene bivergent crustal extension in the Aegean: Evidence from the western Cyclades (Greece). Lithosphere. 4, 23–39, doi.org/10.1130/L164.1

Griffith, A.A., 1921. The phenomena of rupture and flow in solids. Phil.Trans. Roy. Soc. A., 221, 163-198

Griffith, A.A., 1924. The theory of rupture. First international congress of Applied Mathematics, Delft, pp. 55-63

Gudmundsson, A., 1983. Form and dimensions of dykes in eastern Iceland Tectonophysics, 95, 295-307

Gudmundsson, A., 1988. Formation of collapse calderas. Geology, 16, 808-810.

Gudmundsson, A., 1995. The geometry and growth of dykes. In: Baer, G., Heimann, A. (eds), Physics and Chemistry of Dykes. Balkema, Rotterdam, pp.23-34.

Gudmundsson, A., 2002. A. Emplacement and arrest of sheets and dykes in central volcanoes J. Volcanol. Geotherm. Res., 116, 279-298

Gudmundsson, A., 2003. Surface stresses associated with arrested dykes in rift zones Bull. Volcanol. 65, 606-619, 10.1007/s00445-003-0289-7

Gudmundsson A., 2006. How local stresses control magma-chamber ruptures, dyke injections, and eruptions in composite volcanoes Earth Sci. Rev., 79, 1-31.

Gudmundsson, A., 2008. Magma-chamber geometry, fluid transport, local stresses, and rock behaviour during collapse-caldera formation. In: Gottsmann, J., Marti, J. (eds.), Caldera Volcanism: Analysis, Modelling and Response. Developments in Volcanology 10. Elsevier, Amsterdam, pp. 313-349

Gudmundsson, A., 2011a. Deflection of dykes into sills at discontinuities and magma-chamber formation. Tectonophysics, 500, 50–64.

Gudmundsson, A., 2011b. Rock fractures in geological processes. Cambridge University Press, Cambridge.

Gudmundsson, A., 2012. Magma chambers: formation, local stresses, excess pressures, and compartments. J. Volcanol. Geotherm. Res., 237-238, 19–41

Gudmundsson, A., Brenner, S.L., 2001. How hydrofractures become arrested. Terra Nova, 13, 456–462.

Gudmundsson, A., Brenner, S., 2005. On the conditions of sheet injections and eruptions in stratovolcanoes. Bull. Volcanol., 67, 768–782

Gudmundsson, A., Marinoni L.B., Marti J., 1999. Injection and arrest of dykes: implications for volcanic hazards. J. Volcanol. Geotherm. Res. 88, 1-13.

Gudmundsson, A., Philipp, S. L., 2006. How local stress fields prevent volcanic eruptions. J. Volcanol. Geotherm. Res. 158, 257–268.

He, M.Y., Evans A.G, Hutchinson J.W., 1994. Crack deflection at an interface between dissimilar elastic materials. Int. J. Solids Struct. 25,1053-1067.

He, M.Y., Hutchinson, J.W., 1989. Crack deflection at an interface between dissimilar elastic materials. Int J Solids Struct 31, 3443–3455

Heap, M.J., Villeneuve, M., Albino, F., Farquharson, J.I., Brothelande, E., Amelung, F., Got, J-Luc., Baud, P., 2019. Towards more realistic values of elastic moduli for volcano modelling, J. Volcanol. Geotherm. Res. doi: https://doi.org/10.1016/j.jvolgeores.2019.106684

Hutchinson, J.W., 1996. Stresses and failure modes in thin films and multilayers. Technical University of Denmark-Notes for a DCAMM course.

Inglis, C.E., 1913. Stresses in a plate due to the presence of cracks and sharp corners. SPIE Milestone Series, 137, 3-17.

Jaeger, J.C. and Cook N.G.W., 1979. Fundamentals of rock mechanics. Chapman and Hall, London

Jousset, P., H. Mori and H. Okada., 2003. Elastic models for the magma intrusion associated with the 2000 eruption of Usu Volcano, Hokkaido, Japan, J. Volcanol. Geotherm. Res., 125, 81-106.

Kavanagh, J., Menand, T. and Sparks, R., 2006. An experimental investigation of sill formation and propagation in layered elastic media, Earth planet. Sci. Lett., 245, 799–813

Kavanagh, J.L, Rogers, B.D., Boutelier, D., Cruden, A.R., 2017. Controls on sill and dyke-sill hybrid geometry and propagation in the crust: The role of fracture toughness. Tectonophysics, 698, 109-120.

Kavanagh, J.L, Burns, A.J., Hazim, S.H., Wood, E.P., Martin, S.A., Hignett, S., Dennis, D.J.C., 2018. Challenging dyke ascent models using novel laboratory experiments: Implications for

reinterpreting evidence of magma ascent and volcanism, J. Volcanol. Geotherm. Res., 354, 87-101.

Lister, J. R., and Kerr, R. C., 1991. Fluid-mechanical models of crack propagation and their application to magma transport in dykes. J. Geophys. Res. 96, 10049–10077. doi: 10.1029/91JB00600

Le Corvec, N., Menand, T., Lindsay, J., 2013. Interaction of ascending magma with pre-existing crustal fractures in monogenetic basaltic volcanism: an experimental approach. J. Geophys. Res. Solid Earth 118, 968–984.

Le Corvec, N., Muirhead, J.D. & White, J.D.L., 2018. Shallow magma diversions during explosive diatreme-forming eruptions. Nature Communications, 9, 1459, 105 https://doi.org/10.1038/s41467-018-03865-x.

Le Pichon, X., and Angelier, J., 1979. The Hellenic arc and trench system: A key to the neotectonic evolution of the eastern Mediterranean area. Tectonophysics, 60, 1-42

Maccaferri, F., Bonafede, M., Rivalta, E., 2010. A numerical model of dyke propagation in layered elastic media Geophys. J. Int.,180 ,1107-1123

Menand, T., Daniels, K. A., Benghiat, P. 2010. Dyke propagation and sill formation in a compressive tectonic environment, J. Geophys. Res., 115, B08201

Nicholls, I.A., 1971. Petrology of Santorini Volcano, Cyclades, Greece, J. Petrol, 12, 67–119

Parks, M.M., Biggs, J., England, P., Mather, T.A, Nomikou, P., Palamartchouk, K., Papanikolaou, X., Paradissis, D., Parsons, B., Pyle, D.M., Raptakis, C. and Zacharis, V., 2012. 'Evolution of Santorini Volcano dominated by episodic and rapid fluxes of melt from depth. Nature Geoscience, 5, 749-754. doi: 10.1038/NGEO1562

Petersen, A.D.J., 2005. A geological and petrological study of the dikes in the Megalo Vouno volcano complex, Santorini. M.Sc. thesis, Copenhagen University, Denmark

Pollard, D. D. Johnson, A. M., 1973. Mechanics of growth of some laccolithic intrusions in the Henry mountains, Utah, II. Bending and failure of overburden layers and sill formation. Tectonophysics, 18, 311-354

Pinel, V., and Jaupart, C., 2004. Magma storage and horizontal dyke injection beneath a volcanic edifice, Earth Planet. Sci. Lett., 221, 245–262.

Puchelt, H., Hubberton, H. W., Stellrecht, R., 1990. The geochemistry of the radial dykes of the Santorini Caldera and its implications, Thera and the Aegean World III Pro. 3rd Int. Cong., Santorini, Greece, 1989 (D. A. Hardy et al., eds) 229–236 (Thera Found, London 1990)

Ray, R., Sheth, H.C., Mallik, J., 2006. Structure and emplacement of the Nandurbar–Dhule mafic dyke swarm, Deccan Traps, and the tectonomagmatic evolution of flood basalts, Bull. Volcanol. 69, 537-551, doi:10.1007/s00445-006-0089-y

Rivalta, E., Bottinger, M. and Dahm, T., 2005. Gelatine experiments on dike ascent in layered media, J. Volc. Geotherm. Res., 144, 273–285.

Rivalta, E., B. Taisne, A. P. Bunger, R. F. Katz., 2015. A review of mechanical models of dike propagation: Schools of thought, results and future directions, Tectonophysics, 638, 1–42, doi:10.1016/j.tecto.2014.10.003.

Rubin, A.M., Pollard, D.D., 1987. Origins of blade-like dikes in volcanic rift zones R.W. Decker, T.L. Wight, P.H. Stuffer (eds.), Volcanism in Hawaii, US Geological Survey Professional Papers, 1350,1449-1470

Rubin, A. M., 1995. Propagation of magma-filled cracks. Annu. Rev. Earth Planet. Sci. 23, 287–336. doi: 10.1146/annurev.ea.23.050195.001443

Sakellariou, D., Mascle, J., and Lykousis, V., 2013. Strike slip tectonics and transtensional deformation in the Aegean region and the Hellenic arc: Preliminary results. Bulletin of the Geological Society of Greece, 47, 647-656

Scudero, S., De Guidi, G., Gudmundsson, A., 2019. Size distributions of fractures, dykes, and eruptions on Etna, Italy: Implications for magma-chamber volume and eruption potential, Sci. Re, 9, 4139

Sneddon, I.N., 1946. The distribution of stress in the neighbourhood of a crack in an elastic solid. Proceedings of the Royal society doi: 10.1098/rspa.1946.0077

Taisne, B., and Jaupart, C., 2009. Dike propagation through layered rocks, J. Geophys. Res., 114, B09203, doi: 10.1029/2008JB006228.

Tibaldi, A., 2015. Structure of volcano plumbing systems: A review of multi-parametric effects. J. Volcanol. Geotherm. Res. 298, 85-135

Townsend, M.R., Pollard, D.D., Smith, R.P., 2017. Mechanical models for dikes: A third school of thought Tectonophysics, 703-704, 98-118.

Wang L.P and Xu, R., 2006. Dynamic interfacial debonding initiation induced by an incident crack International Journal of Solids and Structures, 43,6535-6550

Xu, R., Huang Y.Y., Rosakis A.J., 2003. Dynamic crack deflection and penetration at interfaces in homogeneous materials: experimental studies and model predictions, Journal of the Mechanics and Physics of Solids, 51, 461-486

Zellmer, G., Blake, S., Vance, D., Hawkesworth, C., Turner, S., 1999. Plagioclase residence times at two island arc volcanoes (Kameni Islands, Santorini, and Soufrière, St. Vincent) determined by Sr diffusion systematics. Contrib. Mineral. Petrol. 136, 345–357